

Modeling of Industrial Pumping System Dynamics

by

Ammar Adnan Al-Nahwi

B.S., Mechanical Engineering
King Saud University (Riyadh), June 1990

Submitted to the Department of Mechanical Engineering
in Partial Fulfillment of the Requirements for the Degree of

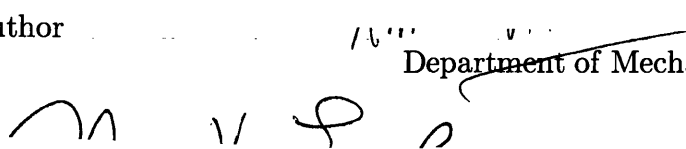
MASTER OF SCIENCE IN MECHANICAL ENGINEERING

at the

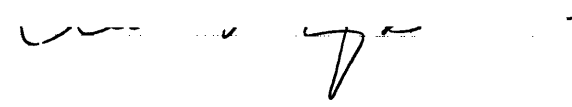
Massachusetts Institute of Technology
February 1996

©1996 Massachusetts Institute of Technology. All rights reserved.

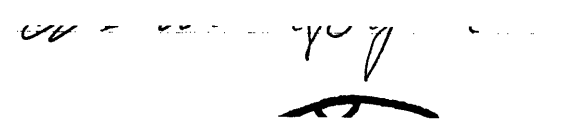
Signature of Author


Department of Mechanical Engineering
December 29, 1995

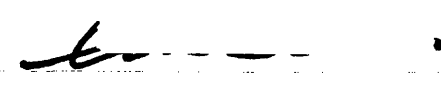
Certified by


Professor Alan H. Epstein
Thesis Supervisor

Certified by


Professor Neville Hogan
Thesis Reader

Accepted by


Ain A. Sonin
Chairman, Departmental Graduate Committee

MASSACHUSETTS INSTITUTE
OF TECHNOLOGY

MAR 19 1996

ENG

LIBRARIES

Modeling of Industrial Pumping System Dynamics

by

Ammar Adnan Al-Nahwi

Submitted to the Department of Mechanical Engineering on December 29, 1995
in Partial Fulfillment of the Requirements for the Degree of
Master of Science in Mechanical Engineering

Abstract

One dimensional, lumped element, analytical models were developed to examine the transient behavior and stability criteria of industrial pumping systems and investigate the underlying physics. This work was motivated by the need to predict and understand the transient behavior of these systems in a manner that would facilitate developing more effective control strategies, designing inherently more stable industrial pumping systems, and minimizing the need for field testing.

A base-line model was first formulated, comprising of a turbine driver, a process compressor, an inlet compressor duct, a process column (plenum) and a compressor discharge valve. The resulting mathematical model was able to capture the system's instability onset point, the non-linear post-stall behavior, and their sensitivity to the system's physical parameters. Two non-dimensional groups were found to play a dominant role in the overall dynamics. Small values of the ratio of fluid compliance to fluid inertia on the compressor side (known as the B -parameter) had a strong stabilizing effect and were associated with high frequency surge oscillations. In contrast, small values of mechanical to fluid inertia ratio had a strong stabilizing effect only in a limited region of the compressor operating range and had little effect on surge frequency. The model explained the stabilizing effect of driver dynamics and its role in initiating the instability mechanism.

The model was expanded to include a driver speed control loop on the turbine side, and a recycle loop on the compressor side, reaching a pumping system of practical complexity. The expanded model allowed for examining realistic transient scenarios such as shut-down and recovery from surge. It was found that the driver speed controller has strong effect on system dynamics during large transients (such as shutdown) but less significant effect on the post-stall behavior. The expanded model provides a means of analyzing the dynamics of a wide class of industrial pumping systems and explaining the physics behind it.

Thesis Supervisor: Professor Alan H. Epstein

Title: Professor of Aeronautics and Astronautics

Acknowledgments

I would like to thank all those who contributed to making the past two years such a rewarding experience. I am grateful to my advisor, Professor Alan H. Epstein, for giving me the opportunity to work with him. His guidance, support and encouragement are deeply appreciated. I am also grateful to Professor Edward M. Greitzer and Professor James D. Paduano for their interest and insightful input. Thanks also to Professor Neville J. Hogan for many useful discussions and for acting as the reader of this thesis.

I would like to thank the Saudi Arabian Oil Company (Saudi Aramco) in general and Abqaiq Plants in particular for providing me with the opportunity and support necessary to pursue my graduate studies. The services provided by the Company's office in Houston are also appreciated. In particular, I am grateful to Mr. Brad Brumfield for his constant encouragement and support.

I would like to thank all the students in the Gas Turbine Laboratory who continue to make my stay pleasant and memorable. Special thanks to: Martin B. Graf for his constant interest, valuable input and for being the sincere friend and neighbor that he is, Jan K. Krasnodebski for many rich technical discussions and a pleasant and lasting friendship, and, John B. Brookfield who together with Jan created the perfect office "environment" each in his own different way. Thanks also to Ken Gordon, Don Hoying, David Tew, and Harald Weigl for very delightful technical, athletic and social interactions.

Last but not least, I am grateful to the compassionate friendship and kindness extended to me by my friends: Fouzi Al-Essa, Mohammad Ali, Mohammad Al-Majed, Isam Habboush, Arshad (Rajesh) Khan, M. Jalal Khan, and Samer Nayfeh.

To my family

I can not think of anybody, next to Allah, more worthy of my gratitude than my parents. Their love, teachings and prayers have been a crucial source of morality and determination through different stages of my life, particularly during the past two years. I hope this effort qualifies to symbolize a partial reward for their infinite giving and sacrifices.

I am indebted to my brother Bilal whose exemplary crave for excellence and unbounded kindness were vital to my emotional and financial stability. My deepest appreciation to my caring sister and her husband for their endless support and encouragement. My highest respect and love to my brother Mohammad for being a dependable man at the age of twelve. The continuous generosity of my parents in law has been significant and is deeply appreciated. Thanks also to my brothers in law, especially for Ibrahim and his entertaining e-mails.

Throughout this journey I have been most fortunate to enjoy the precious company of my beloved wife Nada. To her patience, encouragement, and compassion I credit the success of this journey and the ones to come. My son Majed and my daughter Ayah have provided a more profound meaning to all of this. They, together with their mother, definitely fill my life with joy and make it worthwhile.

This thesis is dedicated to the memory of my brother Eyad (1971-1991).

All praise be to Allah, the most beneficent, the most merciful.

Contents

1. Introduction	17
1.1 Background	17
1.2 Previous Work	20
1.3 Motivation, Objectives and Approach	22
1.4 Organization	25
2. Theoretical Formulation of a Basic Industrial Pumping System Model	27
2.1 Component Off-Design Performance and Constitutive Relations	28
2.1.1 Compressor and Turbine Off-Design Performance	28
2.1.2 Inertance, Compliance and Dissipating Elements Constitutive Relations	34
2.2 Development of the Base-Line Model	35
2.2.1 System Description	35
2.2.2 Formulation of Governing Equations	35
2.2.3 Analysis of Two Special Cases of The Base-Line Model	44
2.2.4 Physical Mechanism of Instability and Interpretation of Stability Criteria	49
3. Simulation and Analysis of a Basic Industrial Pumping System Model	59
3.1 Model without Turbine Speed Control	59
3.1.1 Formulation of Governing Equations	60
3.1.2 Non-dimensionalization of Governing Equations	63
3.1.3 Linear Stability Analysis	66
3.1.4 Simulation of the Non-linear Model	68
3.2 Assessment of Model Assumptions	70

3.2.1	Effect of Driver Efficiency Variations	70
3.2.2	Effect of Compressor Pressure–Rise Time Lag	71
3.3	Model with Turbine Speed Control	73
3.3.1	Formulation of the Speed Governor Control	73
3.3.2	Analysis of the System Model with Speed Control	78
3.4	Discussion of Results	80
4.	Dynamics of Typical Configuration Industrial Pumping System	97
4.1	Typical Pumping Station: Single Compression Train	97
4.1.1	Control Valves and Recycle Lines	97
4.1.2	Incorporating a Recycle Loop in the Model	98
4.1.3	Simulation of The Overall System	101
4.1.4	Discussion of Recycling Performance	102
5.	Summary and Conclusions	109
5.1	Summary and Conclusions	109
5.2	Recommendations For Future Research	111
	References	115

List of Figures

Figure (2.1)	Schematic of the base-line pumping system	53
Figure (2.2)	Typical compressor characteristics: pressure ratio versus mass flow rate for different operating speeds.	53
Figure (2.3)	Typical compressor characteristics: power and efficiency versus Mass Flow Rate for different operating speeds.	54
Figure (2.4)	Low pressure ratio compressor characteristics including the post-stall region, non-dimensionalized by rotor speed [8].	54
Figure (2.5)	Low pressure ratio compressor torque characteristics including the post-stall region, non-dimensionalized by rotor speed [8].	55
Figure (2.6)	Typical turbine characteristics: (a) mass flow rate, horsepower and efficiency versus pressure ratio for different operating speeds at a given inlet pressure [26]. (b) mass flow rate and torque versus rotor speed for a given pressure ratio [2].	56
Figure (2.7)	System operating map: characteristics of compressor and discharge valve illustrating stability of different operating points.	57
Figure (2.8)	Illustration of instability mechanisms.	57
Figure (2.9)	Illustration of instability mechanism including rotor speed variations.	58
Figure (3.1)	Turbine characteristics: (a) mass flow rate–pressure ratio. (b) flow and torque as function of rotor speed. Both for a given turbine inlet pressure.	83
Figure (3.2)	Compressor characteristics: (a) pressure rise–mass flow rate. (b) torque–mass flow rate. Both in dimensional form showing different speed lines.	84
Figure (3.3)	Non-dimensional compressor characteristics: (a) pressure rise coefficient–flow coefficient. (b) torque coefficient–flow coefficient. (eq. 2.16, 17)	85
Figure (3.4)	Discharge valve characteristics: mass flow rate–pressure rise, for different values of ζ_V .	86
Figure (3.5)	Linear stability of base-line model: Effect of B^* and J^* . (a) for $\zeta_V = 2.0$. (b) for different values of ζ_V .	87

Figure (3.6)	Numerical simulation: system response to a step input in $\zeta_V = 1.0$ to 2.0 at $t^* = 4.0$, system parameters: $B^* = 3.15$ and $J^* = 58.44$.	88
Figure (3.7)	Numerical simulation: system response to a step input in $\zeta_V = 1.0$ to 5.0 , at $t^* = 4.0$, system parameters: $B^* = 0.1$ and $J^* = 58.44$.	89
Figure (3.8)	Summary of simulation results: $\zeta_V = 2.1$, Effect of B^* and J^* on post-stall period of oscillation.	90
Figure (3.9)	Turbine flow, torque and efficiency variation with rotor speed.	90
Figure (3.10)	Schematic of system with driver speed control.	91
Figure (3.11)	Simulation: post-stall behavior with no speed control. Step input in $\zeta_V = 1.0$ to 2.5 , at $t^* = 4.0$, $B^* = 3.15$ and $J^* = 0.3$.	92
Figure (3.12)	Simulation: post-stall behavior with speed control. Step input in $\zeta_V = 1.0$ to 2.5 at $t^* = 4.0$, system parameters: $B^* = 3.15$ and $J^* = 0.3$.	93
Figure (3.13)	Simulation: shut-down scenario with high value of governor gain, $K_p = 3.1$. Step input; ω_{ref} set to zero at $t^* = 8.0$. $\zeta_V = 1$ at all times, $B^* = 3.15$, and $J^* = 29.22$.	94
Figure (3.14)	Simulation: shut-down scenario with small value of governor gain, $K_p = 0.31$. Step input; ω_{ref} set to zero at $t^* = 8.0$. $\zeta_V = 1$ at all times, $B^* = 3.15$, and $J^* = 29.22$.	95
Figure (4.1)	Typical configuration of industrial pumping station: single compression train.	105
Figure (4.2)	Typical compressor characteristic map showing the surge line and the safety line used to avoid surge.	105
Figure (4.3)	Schematic of model incorporating a recycle loop.	106
Figure (4.4)	Simulation: model with recycle loop. Effect of K_R . (a) $K_R = 0.436$. (b) $K_R = 0.437$.	106
Figure (4.5)	Simulation: model with recycle loop. Effect of $\tau_{lag,R}$. (a) $\tau_{lag,R} = 5$, $K_R = 0.2$. (b) $\tau_{lag,R} = 5$, $K_R = 0.22$. (c) $\tau_{lag,R} = 0.1$, $K_R = 0.5$.	107

List of Tables

Table (3.1)	Base-line model non-dimensional variables and parameters	64
Table (3.2)	Values of system variables and boundary conditions at design point.	66
Table (3.3)	Values of system physical parameters	66
Table (3.4)	Nominal values of turbine governor sub-system parameters.	78
Table (4.1)	Summary of recycle loop performance indices.	104

Nomenclature

General Variables

A	area, m^2
a	speed of sound, m/sec
B	Greitzer B -parameter
b	damping coefficient, $N/(m/sec)$
b_1, \dots, b_7	coefficients of compressor torque characteristic
C_p	specific heat at constant pressure, Joule/kg K
C_v	specific heat at constant volume, Joule/kg K
c	free constant
c_1, \dots, c_5	coefficients of compressor pressure rise characteristics
d	diameter, m
E	error; difference between reference and instantaneous rotor speed, rad/sec
e_1, e_2	coefficients of turbine mass flow rate–pressure ratio characteristics
F	force, N
f_1, \dots, f_3	coefficients of turbine efficiency characteristics
J	lumped polar mass moment of inertia, $kg \cdot m^2$
K	proportional control gain
k	spring stiffness constant, N/m
k	ratio of specific heats of the turbine fluid
k_t	steam turbine inlet throttle valve coefficient
k_V	coefficient of compressor discharge valve characteristic, $(kg \cdot m)^{-1}$
L	duct length, m
$M_{C,\omega}$	slope of compressor characteristics, $\dot{m}_C(\Delta p, \omega)$, at constant Δp
$M_{C,p}$	slope of compressor characteristics, $\dot{m}_C(\Delta p, \omega)$, at constant ω
$M_{V,p}$	slope of discharge valve characteristic, $\dot{m}_V(\Delta p)$
m	mass, kg
\dot{m}	mass flow rate, kg/sec
P	power, Watt
$P_{C,\omega}$	slope of compressor characteristics, $\Delta p_C(\dot{m}_C, \omega)$, at constant \dot{m}_C
$P_{C,m}$	slope of compressor characteristics, $\Delta p_C(\dot{m}_C, \omega)$, at constant ω

$P_{V,m}$	slope of discharge valve characteristic, $\Delta p(\dot{m}_v)$
p	pressure, Pa
R	gas constant, Joule/kg K
r	radius, m
T	temperature, K
T_D	derivative controller time constant
T_H	Helmholtz resonator period, sec
T_I	integral controller time constant
t	time, sec
u	flow velocity, m/sec
V	volume, m ³
W	work, Joules
x	displacement, m
X	performance index of the recycle loop
y_1, \dots, y_3	intermediate system states, equation (3.30)
z_1, z_2	coefficients of turbine throttle valve characteristics, equation (3.22)

Greek Variables

Γ	non-dimensional torque characteristic function
γ	ratio of specific heats of the compressor fluid
ζ	damping ratio
η	efficiency
π_C	total-to-total compressor pressure ratio ($p_{0,dis} / p_{0,suc}$)
π_T	total-to-total turbine pressure ratio ($p_{0,in} / p_{0,out}$)
ρ	density, kg/m ³
τ	torque, N.m
Φ	non-dimensional mass flow characteristics ($\Phi(\psi) = \Psi^{-1}$)
ϕ	flow coefficient: non-dimensional mass flow rate ($\dot{m} / \rho \omega_d r A$)
ϕ'	flow coefficient: non-dimensional mass flow rate ($\dot{m} / \rho \omega r A$)
Ψ	non-dimensional pressure rise characteristics ($\Psi(\phi) = \Phi^{-1}$)
ψ	pressure rise coefficient: non-dimensional pressure rise ($\Delta p / \rho (\omega_d r)^2$)
ψ'	pressure rise coefficient: non-dimensional pressure rise ($\Delta p / \rho (\omega r)^2$)

ω rotor speed, rad/sec, (also frequency, rad/sec)

Subscripts

0 total (stagnation) property
C compressor
d design point value
d down-stream duct on compressor side
dis compressor discharge
G turbine governor
H Helmholtz resonator parameter
in inlet
out outlet
p plenum
R recycle line parameter
ref reference value (or controller input)
suc compressor suction
T turbine
t turbine throttle
u up-stream duct on compressor side
V discharge valve on compressor side

Superscripts

* non-dimensional group
- averaged quantity

Chapter 1

Introduction

1.1 Background

Industrial pumping systems constitute a critical part of most process industries. Natural gas and crude oil processing plants are typical examples, in which pumping systems are the prime means of transporting the product between different parts of the plant and to the outside world for delivery.

For most applications, these systems are required to withstand uninterrupted operation for extended periods of time. They are also required to shift, smoothly and safely, between different operating conditions to meet various market demands. In addition, these systems should be able to cope with transients produced by other components in the system, such as the start-up of another pumping station or the sudden opening of a valve. In critical applications, where hazardous fluids are involved for example, failure to meet these requirements can be catastrophic. In order to ensure reliable and safe operation of industrial pumping systems, it is important to understand their transient behavior in a way that reflects on their design, operation and control.

Many types of undesirable transient behavior (instabilities) of pumping systems have been reported and investigated. Examples of the most common instabilities are: compressor surge and rotating stall and turbine hunting. The first

two represent unsteady oscillations about a mean operating point, while the latter is a quasi-steady movement of the mean operating conditions.

Compressor surge occurs when the back pressure at the compressor discharge is increased to a certain limit above which the compressor can not withstand the imposed back pressure. As a result, the compressor flow field becomes unstable and the compressor pressure rise capability deteriorates. Downstream components, now at a higher pressure, start to blowdown through the compressor, resulting in large scale reversal in compressor mean flow with a corresponding reduction in back pressure. Once the back pressure becomes sufficiently low, the compressor recovers and begins pumping forward again, thus causing the back pressure to increase and the cycle to repeat. Since most compressors are not designed to endure the cyclic loading that accompanies surge oscillations, few surge cycles can result in severe damage to the compressor internal components.

Another mode of compressor instability is rotating stall. The operating conditions that lead to this instability are very similar to those leading to surge. However, if the system has very small downstream compliance (mass storage capacity), the flow reversal is less likely to occur, and the compressor shifts to another stable operating point at reduced flow and pressure rise. The instability in this case remains local to the compressor internal flow field (with no global flow reversal), yet, it can be very damaging to the compressor.

Turbine hunting, on the other hand, is associated with the turbine speed regulation mechanism. This mechanism is comprised of a controlling device, a governor, and a complex network of mechanical and hydraulic elements. As the load on the turbine changes, the governor detects a corresponding change in shaft speed, and issues a correcting signal. The mechanism then communicates the

signal to the turbine inlet throttle valve, which modulates the turbine mass flow rate and recovers the original operating speed. Due to the presence of damping, compliance and inertia within the governor mechanism, it is possible under certain conditions that this regulatory action develops into a forced instability (resonance) taking the form of sustained oscillations in turbine speed and other system variables.

Although pumping systems in different applications share many features, including some of the instabilities described above, they can be different in many ways. As an example, a compressor within a gas turbine engine can experience surge or stall or both. The major interacting components are the turbine (dissipating throttle), the burner (compliance volume), and the compressor (inertia and pressure rise) which in this case shares the same flow stream with the turbine. In contrast, a process compressor in an industrial application interacts with an independent driver (that has its own flow stream and speed control device), a controlled discharge valve, process components of different sizes and functions, a recycle line and a network of piping. In many configurations, several process compressors are installed to operate in parallel or in series. Further, industrial compressors are designed to handle different fluids and operating conditions.

In order to enhance the stability of pumping systems in general, designers and operators have devised many preventive techniques based on experience and careful observations. Currently, modern control schemes are utilized in managing the operation of industrial pumping systems. Such schemes are designed to prevent the system from operating within or near the pre-defined unstable region by carefully manipulating the system's mean flow, pressure and speed. On-line measurements provide the sensory signals while high speed microprocessors issue

the control signals obtained from complex control algorithms. The controlling action mostly involves the regulation of the recycle line flow and the reduction of system speed. These control systems are custom-built for a particular facility, and are usually based on field testing which may include a surge test.

Recently, analytical models have been developed to predict and quantify the dynamic behavior of simple pumping systems resembling, in most cases, a jet engine. Such models contributed significantly in establishing a more thorough and consistent understanding of the unsteady phenomena of interest [9, 10]. They also allowed for the introduction of new concepts in the field of compression systems stability, such as the “active control of compressor instabilities” and “suppression of compressor instabilities using tailored-structures,” [6, 12].

1.2 Previous Work

Lumped element models have been used over the last forty years to model the dynamics of different compression systems, mostly those of laboratory pumps and compressors or experimental gas turbine engine.

Emmons [5] presented the first successful analogy between Helmholtz resonators and basic surge dynamics. Using a linearized lumped parameter model, he found good agreement between the predicted and measured instability onset point as well as the effect of system parameters on the frequency of oscillation.

Paynter [19] introduced a bond graph representation of Eulerian Turbomachines that captured the main features of real machines, and was consistent with the bond graph modeling notation. Utilizing similarity concepts, he recast the non-linear constitutive relations of a certain class of turbomachines into a Gy-

rator element and a series of Resistor elements. He also demonstrated the use of this notation in examining few simple cases, emphasizing its advantages.

Greitzer [10, 11] examined, both experimentally and analytically, a basic compression system containing a three stage axial compressor. He developed a fourth order non-linear analytical model and quantified the system's post-stall transient behavior through numerical simulations. The ability of the compression system to sustain a limit-cycle behavior (surge) was found to primarily depend on a non-dimensional group called the B -parameter which represents the ratio of compliance to inertia in the system. His experiments showed very good agreement with the theoretical predictions.

Fink [7] performed a similar study using a small turbocharger. His model accounted for rotor speed variations and compressor time lag, and predicted that both have stabilizing effects. He also performed an extensive set of experiments and confirmed his theoretical predictions.

Simon [23] recast the surge model in a form suitable for control applications, and used it to investigate different feedback stabilization techniques to extend the stable operating range of the compressor. He also examined one feedback control scheme experimentally on a centrifugal compressor rig, and showed its benefits over a passive flow restriction in damping the small flow perturbations that precede surge.

A simplified version of Greitzer's surge model was used by Abed, et al. [1] to analyze the non-linear post-stall transient behavior from a bifurcation-theoretic perspective. The role of the B -parameter in controlling the mode of instability was explained using a bifurcation sequence analysis. Two types of post-stall in-

stabilities were detected; namely, sustained oscillations (surge) and unstable oscillations (anti-surge).

McNulty [17] performed an analytical study to assess different sensing and actuation approaches for the suppression of surge as applied to a helicopter gas turbine engine. He used a linearized version of the surge model and assessed the validity of its assumptions in the context of a real gas turbine engine. He showed that, for such an application, heat release in the combustion can have significant effect on engine stability while speed fluctuations had negligible effect.

Rowen [20, 21] presented a simplified mathematical representation of heavy duty gas turbine engines used in General Electric power generation systems. The model included an estimate of system physical and dynamic parameters, such as typical values of time lag for different sensing and actuation components.

1.3 Motivation, Objectives and Approach

Motivation:

Industrial pumping systems can experience different modes of system instability which prevent them from meeting operational and safety requirements. Currently, various designs of control systems are utilized to avoid such instabilities. These designs are based on field surge testing that can potentially be damaging to system components. They also sacrifice efficiency due to excessive recycling, add to the system's complexity, and are not always effective.

The development of a consistent and systematic modeling approach of industrial pumping systems has numerous benefits. It enables the accurate prediction of the transient behavior of industrial pumping systems. Thus, more effective and efficient control schemes may be designed while minimizing the need for field

surge testing. In addition, it leads to the design of more stable pumping systems by providing better insight into the unsteady phenomena. It also facilitates the utilization of the extensive research work performed for different applications involving pumping systems.

This work is a step towards achieving these goals.

Objectives:

The objectives of this work were identified as follows:

- Develop mathematical models that capture the main modes of system instability and predict the transient behavior of industrial pumping systems.
- Assess the validity and limitations of different modeling assumptions, such as constant turbine efficiency and quasi-steady compressor behavior.
- Assess the role of various elements in an industrial pumping system, such as the driver, rotor inertia, and speed regulation devices, on the overall system dynamics.
- Quantify the stability criteria for a basic industrial pumping system.
- Quantify the non-linear system behavior during instability (e.g. compressor surge and turbine hunting oscillations).
- Utilize the simple models developed herein to examine the transient behavior of typical integrated configurations of industrial pumping systems at a practical level of complexity.

Approach:

The modeling work in this thesis is based on extending existing models such as those developed for a gas turbine engine. In order to account for the many differ-

ences between those applications and the ones considered in this study, the models will be reconstructed to include new elements and effects that contribute to the system dynamics. One such element is the independent driver, typically a turbine, that provides the mechanical power to the compressor. Unlike previous studies, a more sophisticated model of a turbine driver is introduced. In addition, the turbine speed control regulation mechanism is also incorporated at a later stage. After the basic model of an industrial pumping system is introduced and analyzed, other typical components are added to the model, which at that point approaches a level of complexity similar to that of actual systems.

The methodology of lumped element (network) modeling is employed throughout this work. Inertial, capacitive and dissipative effects are lumped into idealized elements that represent specific behavior of actual system components. The constitutive relations of these elements are assumed to be available as an input to the model. In practice, these relations can be obtained by actual field testing or from vendors. In this study, the behavior of these components is represented by simple mathematical functions designed to match actual performance data in terms of the main trends and critical features.

The following tools are utilized in analyzing the models. Non-linear simulations are used to examine the transient system response when large variations and disturbances are involved, in which case the non-linear nature of system components are important. Linearized models are also utilized to predict the stability of various operating points. In both linear and non-linear analysis, the effects of different system parameters are examined. A few simple models are examined analytically in an attempt to reveal some general aspects of their dynamic behavior.

Scope:

Industrial pumping systems exist in countless configurations, sizes and services, each of which can potentially have different dynamics. The emphasis in this study is on developing a systematic modeling approach that can be extended to include the diversity of existing systems.

1.4 Organization

This thesis is organized in the following manner. Chapter 1 introduces the subject of industrial pumping systems transient behavior and stability. Pumping systems in different applications are briefly compared from that perspective. Various types of instabilities are described. The motivations, objectives and approach of this work are discussed.

In Chapter 2, the theoretical formulation of a basic industrial pumping system model is presented. The constitutive relations of system components are first discussed in some detail. The modeling assumptions and governing equations are then developed. Two special cases of the basic model are analyzed in a qualitative fashion, allowing for the mechanisms of instability to be physically described.

Chapter 3 presents an extensive analysis of the basic model developed earlier. Specific forms of component constitutive relations are introduced. A steady state analysis is performed which yields a typical industrial pumping system that is fully described. The system's response to disturbances of finite magnitude is examined through non-linear simulations, while the stability of various operating points under small perturbations is examined through linear stability analysis techniques. The effect of system parameter variation on system stability is also investigated. Different modeling assumptions are validated and the main obser-

variations are discussed. Finally, the driver speed control sub-system is incorporated in the model and the dynamics of the new model are examined.

Chapter 4 discusses the role of additional components in the dynamics of typical industrial pumping systems. The model developed earlier is augmented with a recycle loop and the system governing equations are updated accordingly. The dynamics of the overall system are examined through numerical simulations, and the main observations are discussed.

In Chapter 5, the summary and conclusions of the study are presented and recommendations for future work are suggested.

Chapter 2

Theoretical Formulation of a Basic Industrial Pumping System Model

In this chapter, the theoretical formulation of a model that describes the dynamics of a simple industrial pumping system is presented. The system consists of a turbine driver, rotor inertia, compressor inlet duct, process compressor, plenum, and a discharge valve. The formulation yields a third order mathematical description that serves as the base-line model of industrial pumping systems. Two second order models are also examined as special cases—the first recovers the simplest form of Greitzer’s surge model by considering the limit of infinite rotor shaft inertia, while the second considers the limit of negligible fluid inertia in the compressor inlet duct. Both models have the advantage of being amenable to analytical investigation, yet, they capture the main features of the system’s underlying physics.

To achieve this, the performance characteristics of the individual components are first discussed. The modeling assumptions are established and the system dynamic equations are developed. The linear stability of the resulting models is then analyzed using a primarily qualitative approach. Finally, the physical mechanism of instability is described. In the next chapter, the model will be extended further to include other characteristic features of more complex industrial pumping systems.

2.1 Component Off-Design Performance and Constitutive Relations

2.1.1 Compressor and Turbine Off-Design Performance

Background:

The dynamics of the overall system are largely influenced by the off-design performance characteristics of the individual components, usually presented in the form of pressure ratio–mass flow rate maps. A less common, but equally important, representation for a turbomachine is the maps of torque and power characteristics as a function of mass flow rate and rotor speed. These maps describe the constitutive relations whereby different system variables are related across any given element. They are analogous to Hooke’s law for a compliance element in mechanical springs or Ohm’s law for an electrical resistance, except that for a turbomachine these relations have a more complex and non-linear nature. Such complexity is the result of the complicated flow field and geometry within the turbomachine.

For design purposes, the performance characteristics can be predicted using advanced Computational Fluid Dynamics techniques, which is an active area of research, or alternatively, using empirical methods based on previously tested machines. For the purposes of the current study, it is sufficient to represent the characteristic maps by simple mathematical relations provided that they capture the general trends and critical features of real machines. The specific forms of these relations are introduced in the following chapter.

In general, the constitutive relations of a compressor handling a compressible single gas flow can be expressed in a functional form using dimensional analysis [4, 13].

Neglecting the effects of Reynolds number and dropping fixed geometric parameters, these relations can be written as,

$$\frac{p_{0,dis}}{p_{0,suc}}, \eta_C, \frac{\Delta T_{0,C}}{T_{0,suc}} = f\left(\frac{\dot{m}_C \sqrt{T_{0,suc}}}{p_{0,suc}}, \frac{N}{\sqrt{T_{0,suc}}}\right), \quad (2.1)$$

where, $p_{0,suc}$ and $p_{0,dis}$ are the total pressure at the compressor suction and discharge stations respectively, η_C is the compressor efficiency, $\Delta T_{0,C} = T_{0,dis} - T_{0,suc}$ is the total temperature rise across the compressor, \dot{m}_C is the mass flow rate through the compressor and N is the rotor speed (rev/min).

Assuming constant conditions at the compressor suction and replacing the temperature ratio with the power and torque, this becomes,

$$\pi_C, \eta_C, P_C, \tau_C = f(\dot{m}_C, \omega). \quad (2.2)$$

where, π_C , P_C and τ_C are the compressor pressure ratio, power consumption and torque respectively, and ω is the rotor speed (rad/sec). It is useful to note that, based on assumptions introduced below, only two of these four functions need to be specified or determined experimentally, from which the other characteristic functions can be derived. Figure (2.2) shows a typical example of the characteristics described by equation (2.1).

For a turbine, it is common to consider the mass flow rate to depend on the rotor speed and pressure ratio. Therefore, the constitutive relations of a turbine can be written as [14],

$$\frac{\dot{m}_T \sqrt{T_{0,in}}}{p_{0,in}}, \eta_T, \frac{\Delta T_{0,T}}{T_{0,in}} = f\left(\frac{N}{\sqrt{T_{0,in}}}, \frac{p_{0,in}}{p_{0,out}}\right), \quad (2.3)$$

where, the subscript T indicates a quantity on the turbine side, and the subscripts in and out refer to the turbine inlet and outlet stations respectively.

The turbine constitutive relations can also be simplified by fixing the inlet conditions,

$$\dot{m}_T, \eta_T, P_T, \tau_T = f(\omega, \pi_T). \quad (2.4)$$

In the context of system dynamics, it is particularly helpful to specify the input and output variables for a given element; i.e. to indicate which variables are imposed by the system and which are imposed by the element itself. For most resistive elements, such a specification (referred to as causality assignment) can be a matter of mathematical convenience. However, for capacitances, inertances, and resistances with non-single valued constitutive relations, the input-output specification may reflect different boundary conditions and possibly different dynamics. This issue can be made clearer by considering two different turbomachines; a compressor and a turbine. For a given compressor, the mass flow rate and rotor speed are imposed by system boundary conditions (e.g. suction pressure, discharge valve set-point) and the rotor torque balance respectively, while the compressor responds with a corresponding pressure rise. However, for a given turbine, it is the pressure drop and the rotor speed, imposed also by the system boundary conditions and torque balance, that set the mass flow rate through the turbine.

In physical terms, the difference between the compressor and the turbine constitutive relations comes from the fact that within a compressor the work is done

by the impeller (or blades) on the fluid, thus producing an increase in the energy content of the fluid in the form of pressure and temperature rise. The amount of energy transmitted, and hence the pressure and temperature rise, are all dependent on the speed of the rotor and the rate of mass flowing through it. In the case of a turbine, the energy is transmitted from the fluid to the rotor. The pressure difference between the inlet and outlet represents the potential that drives the flow, while the internal flow path through the turbine represents the resistance to the flow. Therefore, the mass flow rate, and hence the amount of energy transmitted, are controlled primarily by the pressure difference and flow resistance—the latter being influenced by the rotor speed since moving parts within the turbine act to increase the equivalent flow resistance. The effect of rotor speed on the turbine mass flow rate is not substantial in regions of operation close to the design point, nevertheless, changes in rotor speed have a more significant influence on the turbine efficiency, power and torque [2, 26].

Simplification of Compressor and Turbine Characteristics:

In many practical cases, the constitutive relations of a turbomachine can be simplified even further. For example, the flow in a low pressure ratio, low speed compressor can be regarded as incompressible for which dimensional analysis leads to the following functional form of the compressor characteristics [4],

$$\frac{\Delta p_C}{\rho_C (\omega r)^2} = \Psi_C \left(\frac{\dot{m}_C}{\rho_C \omega r A_u} \right), \quad (2.5)$$

or,

$$\Delta p_C = \rho_C (\omega r)^2 \Psi_C \left(\frac{\dot{m}_C}{\rho_C \omega r A_u} \right), \quad (2.6)$$

where, $\Delta p_C = p_{0,dis} - p_{0,suc}$, is the compressor steady state total pressure rise, ρ_C is the density of the compressor flow, and Ψ_C is the non-dimensional compressor pressure rise characteristic function. Defining non-dimensional pressure rise and mass flow rate as $\psi'_C = \Delta p_C / (\rho_C \omega^2 r^2)$ and $\phi'_C = \dot{m}_C / (\rho_C \omega r A_u)$ respectively¹, equation (2.5) can be rewritten as,

$$\psi'_C = f(\phi'_C). \quad (2.7)$$

In this form, the rotor speed does not appear explicitly in the relation, which is convenient whenever the rotor speed variations are small or unimportant. All the speed lines in Figure (2.2) collapse to a single curve and the compressor becomes a single port element with ψ'_C and ϕ'_C as the effort and flow variables² respectively. Figure (2.4) is a typical example of such a presentation.

The compressor power and torque consumption can be estimated using simple control volume analysis. Assuming an adiabatic machine with no mass storage capacity, the first law of thermodynamics as applied to an open system (the compressor in this case) can be written as,

$$P_C = \omega \cdot \tau_C = \dot{m}_C C_v \Delta T_C(\dot{m}_C, \omega) + \frac{\dot{m}_C}{\rho_C} \Delta p_C(\dot{m}_C, \omega), \quad (2.8)$$

¹ The same symbols, ϕ_C and ψ_C without the prime, will be used in the next chapter to indicate a slightly different definition—the rotor speed at design point, ω_d , will be used for non-dimensionalization instead of ω . The reason is that ω will be a state variable in the formulation. The prime is used here to differentiate between the two.

² Effort and Flow variables are standard terminology in the bond graph notation used to model dynamic networks. Each interaction between two elements in the system involving power exchange is represented by a bond. Each bond is usually associated with an effort and a flow variable such that their product is always the power transmitted through that bond. In mechanical systems, for example, these would be the force and velocity respectively. The compressor can be treated as a single port element if the speed is assumed constant. Reference [19] introduces a bond graph representation and a few applications of incompressible turbomachines. Reference [15] provides a full coverage of the bond graph theory.

where $\Delta T_C(\dot{m}_C, \omega)$ is a characteristic of the compressor. Since the torque characteristics will be required as an input in the following formulation, it can be directly specified based on experimental data.

For the turbine, the assumption of constant rotor speed simplifies the constitutive relation in a similar manner and allows the turbine to be modeled as a throttle valve or even as a one dimensional compressible nozzle (usually choked). Another simplification can be introduced by assuming constant pressure drop for a turbine with no mass flow rate modulation. As the assumption of constant rotor speed may be suitable for modeling a turbine within a jet engine [10, 17], it may not be as suitable for an independent driver such as an industrial turbine. The second assumption, however, is more applicable in the case of industrial turbines as will be shown below.

Typical Compressor and Turbine Performance Maps:

Figure (2.2) through Figure (2.6) show typical performance characteristics of compressors and turbines. Figure (2.2) is a typical compressor performance map showing pressure ratio and efficiency as a function of flow rate. The pressure rise curves (referred to as speed lines) terminate at the surge line where the compressor flow field becomes unstable at such reduced mass flow rates, resulting in significant deterioration of the compressor's pressure rise capabilities. The shape of the speed lines to the left of the surge limit, including reversed flow conditions, may be experimentally determined by appropriate averaging of transient performance data [7, 8, 11]. In this study, the compressor characteristics, including the post-stall region, will be approximated using simple mathematical functions (typically quadratic polynomials). Figure (2.3) shows compressor power and efficiency as a function of mass flow rate for different rotor speeds. Figure (2.4) and Figure (2.5)

show actual compressor pressure rise and torque characteristics respectively. Both maps are presented in the form suggested by equation (2.5) and (2.17).

Figure (2.6)a is a typical turbine performance map showing the mass flow rate versus the pressure drop for different rotor speeds. Two observations can be made from the Figure; that an increase in the rotor speed results in a decrease of mass flow rate for a given pressure drop, and that the maximum mass flow rate is limited by choking at some critical value of the pressure drop, which in turn depends on the number of turbine stages. Figure (2.6)b is a different presentation of turbine performance characteristics, in which the mass flow rate, efficiency and torque are plotted against rotor speed for a given pressure drop. It can be seen from the Figure that as the rotor speed is varied between the two extremes, the mass flow rate varies only between 80–140% of the design point value whereas the torque and efficiency vary between 0–300% and 0–100% respectively.

2.1.2 Inertance, Compliance and Dissipating Elements Constitutive

Relations

Two types of inertance elements are considered: mechanical and fluid inertia. The constitutive relation for either is Newton's second law in its linear or angular form. The compliance elements, on the other hand, are mostly fluid in which the compression and expansion processes are assumed to follow a thermodynamic relation that most closely describe the actual process, such as the isentropic process relation.

The dissipating elements, such as the compressor discharge valve, are also fluid and their constitutive relations are typically non-linear, empirically determined functions relating mass flow rate to pressure drop. Bernoulli's equation is some-

times used to represent the constitutive relation of such an element by dropping the inlet kinetic energy term to account for the losses in the throttling process. Such a crude approximation may be accepted provided that the pressure drop across the throttle is small enough for the flow to be considered incompressible.

2.2 Development of the Base-Line Model

2.2.1 System Description

The considered system is shown in Figure (2.1). It consists of a turbine which receives high pressure and temperature gas (typically steam) and converts its high thermal energy content to mechanical torque at the rotor coupling. The gas leaves the turbine at a much lower pressure and temperature. The rotor, which represents the mechanical inertia element, drives a low pressure-ratio compressor that receives low pressure and temperature gas (typically natural gas) from the suction duct, which represent the fluid inertia element, and discharges it at a higher pressure and temperature. The gas then passes through a relatively large volume component, the plenum, that represents the fluid compliance element in the system. The plenum may correspond to different process components in an actual plant, such as condensate removing drums or separation columns. The considered system ends with a compressor discharge valve that maintains the required compressor back pressure during steady state and sets the overall system operating point.

2.2.2 Formulation of Governing Equations

For a lumped parameter model to capture an oscillatory phenomenon, such as compressor surge, it has to have at least one equivalent inertia element and one

equivalent compliance element. Greitzer’s surge model [10], which assumes constant rotor speed, models the fluid in the compressor duct and in the plenum as the inertia and compliance elements respectively. Since the driver dynamics are of interest in analyzing industrial systems, the following formulation introduces the rotor shaft into the model as an additional inertia element. Further, a special case that assumes the fluid inertia to be very small and the rotor polar moment of inertia as the main inertia element is also discussed in order to emphasize the role of rotor inertia and driver dynamics. Another special case is considered in which the limit of infinite rotor inertia is assumed. This yields a second order model that solely describes the compressor side and eliminates the driver dynamics.

Driver Model:

The turbine inlet total pressure and temperature are considered constant. At the turbine outlet, a typical assumption is constant static pressure. However, if the outlet gas velocity is relatively low, the total and static outlet pressures are approximately equal, and hence constant. As a result, all turbine characteristics, namely \dot{m}_T , η_T , P_T and τ_T , are functions of rotor speed only. Two of these characteristics need to be specified to describe the performance of the turbine, for example,

$$\dot{m}_T = \dot{m}_T(\omega), \tag{2.9}$$

and,

$$\tau_T = \tau_T(\omega), \tag{2.10}$$

Typical examples of such characteristics are shown in Figure (2.6).

Other assumptions regarding the turbine model include the following: adiabatic, irreversible, quasi-steady expansion process, dry gas at both inlet and outlet, incompressible flow in the inlet and outlet pipes (low Mach numbers),

negligible fluid capacitance and inertia within the turbine, negligible mechanical losses, no gas extraction and negligible gas leakage.

Rotor Model:

In this formulation the rotor includes the turbine and compressor rotating elements as well as a coupling device with no speed reduction.

Neglecting mechanical losses in the bearings and assuming a rigid rotor, the conservation of angular momentum can be written as,

$$J \frac{d\omega}{dt} = \tau_T - \tau_C, \quad (2.11)$$

where J is the equivalent polar moment of inertia of the total rotating assembly.

Compressor Inlet Duct Model:

The flow in the compressor inlet duct is assumed to be one-dimensional, incompressible (low Mach number) and inviscid. It is further assumed that the flow is uniform over the cross section of the duct and is not affected by any non-axisymmetric flow field produced by the compressor. The total pressure at the duct inlet is considered to be a constant boundary set by upstream components, $p_{u,in} = \text{constant}$, whereas the duct total outlet pressure is assumed to be equal to the compressor suction pressure, $p_{u,out} = p_{0,suc}$.

Based on these assumptions, the mass continuity as applied to the duct flow shows that the instantaneous inlet mass flow rate is equal to that at the duct exit and also through the compressor,

$$\dot{m}_{u,in} = \dot{m}_{u,out} = \dot{m}_C = \rho_u A_u u_u, \quad (2.12)$$

where A_u is the cross sectional area of the duct, ρ_u is the constant fluid density in the duct, and u_u is the instantaneous axial flow velocity within the duct. The axial momentum equation can be written for the duct flow as,

$$\left(p_{u,in} - p_{u,out}\right)A_u = \rho_u A_u L_u \frac{du_u}{dt}, \quad (2.13)$$

which can be rewritten using equation (2.12) in terms of mass flow rate,

$$\frac{d\dot{m}_C}{dt} = \frac{A_u}{L_u} \left(p_{u,in} - p_{u,out}\right). \quad (2.14)$$

Finally, the pressure differences $\Delta p_C = p_{0,dis} - p_{0,suc} = p_p - p_{u,out}$, and $\Delta p = p_p - p_{u,in} = p_p - p_{u,out}$, are introduced to yield,

$$\frac{d\dot{m}_C}{dt} = \frac{A_u}{L_u} \left(\Delta p_C(\dot{m}_C, \omega) - \Delta p \right). \quad (2.15)$$

Compressor Model:

The compressor considered in this initial model is a low pressure ratio compressor through which the flow of an ideal gas may be regarded as incompressible. Initially, it is assumed that the instantaneous pressure rise during a transient follows the compressor steady state characteristics described earlier. This assumption is commonly referred to as the quasi-steady assumption, and the compressor is said to be an actuator disk.

Other assumptions regarding the compressor include the following: negligible fluid inertia and compliance (mass storage) within the compressor, adiabatic irreversible compression process, and negligible mechanical losses.

Following the arguments presented in the previous section, the compressor pressure rise and torque characteristics are independently specified as,

$$\frac{\Delta p_C(\dot{m}_C, \omega)}{\rho_C (\omega r)^2} = \Psi_C \left(\frac{\dot{m}_C}{\rho_C \omega r A_u} \right), \quad (2.16)$$

and,

$$\frac{\tau_C(\dot{m}_C, \omega)}{\rho_C (\omega r)^2 r A_u} = \Gamma_C \left(\frac{\dot{m}_C}{\rho_C \omega r A_u} \right), \quad (2.17)$$

from which the compressor power consumption may be obtained,

$$P_C = \omega \tau_C(\dot{m}_C, \omega). \quad (2.18)$$

Plenum Model:

The fluid in the plenum is assumed to have spatially uniform properties and negligible velocity. Further, the compression and expansion processes within the plenum are assumed to follow the isentropic relation,

$$\frac{p_p}{\rho_p^\gamma} = \text{constant}, \quad (2.19)$$

where, p_p is the gas pressure in the plenum, which is equal to the compressor discharge pressure $p_{0,dis}$, ρ_p is the fluid density in the plenum, and γ is the ratio of specific heats for the gas being pumped. Differentiating equation (2.19) and utilizing the ideal gas law,

$$dp_p = \frac{\gamma p_p}{\rho_p} d\rho_p = \gamma R T_p d\rho_p = a_p^2 d\rho_p, \quad (2.20)$$

where, R is the gas constant, T_p is the fluid temperature in the plenum (approximately equal to compressor discharge total temperature), and a_p is the local speed of sound. The compressor temperature rise is relatively small so the variations in the discharge total temperature, and thus the plenum temperature, are even smaller; and hence negligible (see [10, 11] for detailed argument regarding this assumption), i.e.,

$$\gamma R T_p \approx \gamma R T_{0,suc} = \text{constant} = a^2, \quad (2.21)$$

where, a is the speed of sound based on the conditions at the suction. Therefore, the pressure and density in the plenum can be related through,

$$dp_p = a^2 d\rho_p, \quad (2.22)$$

The mass continuity equation for the fixed volume plenum can be written as,

$$V_p \frac{d\rho_p}{dt} = \dot{m}_C - \dot{m}_V, \quad (2.23)$$

which, utilizing equation (2.22), can be written in terms of plenum pressure,

$$\frac{V_p}{a^2} \frac{dp_p}{dt} = \dot{m}_C - \dot{m}_V, \quad (2.24)$$

where, V_p is the volume of the plenum, and \dot{m}_V is the mass flow rate leaving the plenum through the compressor discharge valve. It is convenient to write the above equation in terms of pressure difference, namely $\Delta p = p_p - p_{u,in}$, instead of the plenum pressure, p_p ,

$$\frac{d(\Delta p)}{dt} = \frac{a^2}{V_p} (\dot{m}_C - \dot{m}_V). \quad (2.25)$$

Compressor Discharge Valve Model:

The flow through the discharge valve may be treated as incompressible provided that the pressure drop across the valve is small enough for such an assumption to be made. Fluid inertia and unsteady effects are also assumed negligible.

The mass flow rate through the valve can be expressed in a functional form as,

$$\dot{m}_V = \dot{m}_V(\Delta p_V, k_V), \quad (2.26)$$

where, $\Delta p_V = p_p - p_{V,out}$, is the pressure drop across the valve, $p_{V,out}$ is the constant pressure (boundary condition) downstream the discharge valve, and k_V is a discharge coefficient that depends on the valve opening set-point. Another simplifying, but not necessary, assumption is to consider the compressor duct inlet pressure, $p_{u,in}$, equal to that at the system exit, $p_{V,out}$, in which case Δp_V is equal to Δp (and also equal to Δp_C during steady state). The discharge valve mass flow rate can thus be written as,

$$\dot{m}_V = \dot{m}_V(\Delta p, k_V). \quad (2.27)$$

Figure (3.4) shows an example of a typical valve map with different opening set-points.

System Model:

The overall system dynamics are governed by the equations of angular momentum, axial momentum and mass conservation as applied to the rotor, inlet duct and plenum respectively. Incorporating the constitutive relations for different elements, given by equations (2.10), (2.17), (2.6) and (2.27), the resulting set of non-linear ordinary differential equations become,

$$\frac{d\omega}{dt} = \frac{1}{J} \left[\tau_T(\omega) - \tau_C(\dot{m}_C, \omega) \right], \quad (2.28)$$

$$\frac{d\dot{m}_C}{dt} = \frac{A_u}{L_u} \left[\Delta p_C(\dot{m}_C, \omega) - \Delta p \right], \quad (2.29)$$

$$\frac{d(\Delta p)}{dt} = \frac{a^2}{V_p} \left[\dot{m}_C - \dot{m}_V(\Delta p) \right]. \quad (2.30)$$

The states are the rotor speed, ω , and the compressor mass flow rate, \dot{m}_C , associated with the mechanical and fluid inertia type of energy storage ele-

ments, and the plenum pressure expressed in terms of the pressure difference $\Delta p = p_p - p_{u,in}$, associated with the capacitive type of energy storage elements. Four non-linear constitutive relations are required as an input to the model.

Linearization of Base-Line Model Equations:

Following the standard linearization technique for autonomous, first order, non-linear, continuous systems [18], the linearized version of the model may be formulated using Taylor's series expansion about some steady state operating point, say $(\omega_o, \Delta p_o, \dot{m}_{C_o})$ where all the derivatives with respect to time are identically zero. Assuming $\tilde{\omega}$, $\tilde{\dot{m}}_C$ and $\Delta\tilde{p}$ to be small perturbations around the operating point, the linearized system equations can be written as,

$$\frac{d\tilde{\omega}}{dt} = \frac{1}{J} \left[\left. \frac{\partial \tau_T}{\partial \omega} \right|_o - \left. \frac{\partial \tau_C}{\partial \omega} \right|_o \right] \tilde{\omega} - \frac{1}{J} \left. \frac{\partial \tau_C}{\partial \dot{m}_C} \right|_o \Delta\tilde{p}, \quad (2.31)$$

$$\frac{d\tilde{\dot{m}}_C}{dt} = \frac{A_u}{L_u} \left[\left. \frac{\partial(\Delta p_C)}{\partial \omega} \right|_o \tilde{\omega} + \left. \frac{\partial(\Delta p_C)}{\partial \dot{m}_C} \right|_o \tilde{\dot{m}}_C - \Delta\tilde{p} \right], \quad (2.32)$$

$$\frac{d(\Delta\tilde{p})}{dt} = \frac{a^2}{V_p} \left[\tilde{\dot{m}}_C - \left. \frac{\partial \dot{m}_V}{\partial(\Delta p)} \right|_o \Delta\tilde{p} \right], \quad (2.33)$$

where all the partial derivatives are evaluated at the operating point.

The following notation is used to denote the partial derivatives in the above equations. For instance, derivatives of the turbine and compressor torque functions are denoted as $\mathbf{T}_{T,\omega}$ and $\mathbf{T}_{C,\omega}$ respectively, where the first subscript refers to the component and the second subscript refers to the independent variable, ω in this case, used as basis of differentiation. Similarly, the following parameters may

be defined. $\mathbf{T}_{C,m} = \partial \tau_C / \partial \dot{m}_C$, $\mathbf{P}_{C,\omega} = \partial(\Delta p_C) / \partial \omega$, $\mathbf{P}_{C,m} = \partial(\Delta p_C) / \partial \dot{m}_C$, and $\mathbf{M}_{V,p} = \partial \dot{m}_V / \partial(\Delta p_C)$.

The linearized system equations are then written in the standard matrix form, $(\dot{\mathbf{x}} = \mathbf{A} \mathbf{x})$, in the absence of external forcing as,

$$\frac{d}{dt} \begin{bmatrix} \tilde{\omega} \\ \tilde{\dot{m}}_C \\ \Delta \tilde{p} \end{bmatrix} = \begin{bmatrix} \frac{1}{J} (\mathbf{T}_{T,\omega} - \mathbf{T}_{C,\omega}) & -\frac{1}{J} \mathbf{T}_{C,m} & 0 \\ \frac{A_u}{L_u} \mathbf{P}_{C,\omega} & \frac{A_u}{L_u} \mathbf{P}_{C,m} & -\frac{A_u}{L_u} \\ 0 & \frac{a^2}{V_p} & -\frac{a^2}{V_p} \mathbf{M}_{V,p} \end{bmatrix} \begin{bmatrix} \tilde{\omega} \\ \tilde{\dot{m}}_C \\ \Delta \tilde{p} \end{bmatrix}. \quad (2.34)$$

The coefficients of the characteristic polynomial³ are given by,

$$\begin{aligned} a_2 &= - \left(\frac{A_u}{L_u} \mathbf{P}_{C,m} + \frac{1}{J} (\mathbf{T}_{T,\omega} - \mathbf{T}_{C,\omega}) - \frac{a^2}{V_p} \mathbf{M}_{V,p} \right), \\ a_1 &= \frac{1}{J} (\mathbf{T}_{T,\omega} - \mathbf{T}_{C,\omega}) \left(\frac{A_u}{L_u} \mathbf{P}_{C,m} - \frac{a^2}{V_p} \mathbf{M}_{V,p} \right) \\ &\quad + \frac{A_u}{L_u} \left(\frac{1}{J} \mathbf{P}_{C,\omega} \mathbf{T}_{C,m} + \frac{a^2}{V_p} (1 - \mathbf{P}_{C,m} \mathbf{M}_{V,p}) \right), \\ a_0 &= - \frac{a^2 A_u}{V_p L_u J} \left[(\mathbf{T}_{T,\omega} - \mathbf{T}_{C,\omega}) (1 - \mathbf{P}_{C,m} \mathbf{M}_{V,p}) - \mathbf{P}_{C,\omega} \mathbf{T}_{C,m} \mathbf{M}_{V,p} \right], \end{aligned} \quad (2.35)$$

and must satisfy the following conditions to ensure that all the roots have negative real parts: $a_2 > 0$, $a_1 > 0$, $a_0 > 0$, $a_2 a_1 > a_0$. Unfortunately, further *analytical* investigation of the system at this point results in complex stability conditions

³ The characteristic polynomial may be obtained from $\det(\mathbf{A} - \lambda \mathbf{I}) = 0$, and for a third order system it takes the form $\lambda^3 + a_2 \lambda^2 + a_1 \lambda + a_0 = 0$. The linear stability of the operating point of interest can be examined by testing the roots of the characteristic polynomial, or alternatively by testing the coefficients a_2 , a_1 and a_0 according to the Routh-Hurwitz criterion [18].

that do not shed much light on the physics of the system. Instead, the conditions described above will be considered again in the next chapter when the system parameters are assigned typical numeric values. Nevertheless, the analytical approach can be utilized to examine two special cases of the base-line model; namely, the limit of infinite rotor inertia ($J \rightarrow \infty$), and the limit of negligible fluid inertia in the compressor duct ($L_u \rightarrow 0$).

2.2.3 Analysis of Two Special Cases of The Base-Line Model

Case 1: Infinite Rotor Inertia

This assumption implies that the rotor inertia response to torque differences is much slower and less significant than the dynamics of the rest of the system. From equation (2.28), as J approaches infinity the time derivative $d\omega/dt$ vanishes and the rotor speed, ω , becomes a constant. The resulting simple model, now represented by equations (2.29) and (2.30), is analogous to the basic fluid oscillator known as the Helmholtz Resonator. Different forms of this model have been investigated and utilized by many authors [3, 5, 9, 10, 16, 17]. A summary of this system's stability analysis is presented for comparison purposes with the next case.

The characteristic polynomial⁴ is obtained from the linearized system equations (the second and third in (2.34)) as,

⁴ The standard form of the characteristic polynomial for a second order system is given by $\lambda^2 + (2\zeta\omega_n)\lambda + (\omega_n)^2 = 0$, where ω_n is the undamped natural frequency and ζ is the damping ratio. The stability is determined by the sign of the coefficient of λ and the constant coefficient. Both $(2\zeta\omega_n)$ and $(\omega_n)^2$ must be greater than zero to satisfy the conditions of dynamic and static stability respectively—the former being associated with the rates of feeding and dissipating energy from the system while the latter being associated with the balance of efforts (i.e. forces, pressures or torques) within the system.

$$\lambda^2 + \left(\frac{a^2}{V_p} \frac{1}{\mathbf{P}_{V,m}} - \frac{A_u}{L_u} \mathbf{P}_{C,m} \right) \lambda + \frac{a^2 A_u}{V_p L_u} \left(1 - \frac{\mathbf{P}_{C,m}}{\mathbf{P}_{V,m}} \right), \quad (2.36)$$

where, $\mathbf{P}_{V,m} = 1/\mathbf{M}_{V,p}$ is the slope of the discharge valve characteristic, $\Delta p(\dot{m}_v, \omega)$. This yields the following dynamic and static stability conditions respectively,

$$\mathbf{P}_{C,m} < \frac{a^2 L_u}{V_p A_u} \frac{1}{\mathbf{P}_{V,m}}, \quad (2.37)$$

$$\mathbf{P}_{C,m} < \mathbf{P}_{V,m}, \quad (2.38)$$

From these conditions, it can be shown that:

- the dynamic stability limit is reached before the static stability limit as the operating point is moved from right to left by reducing the mass flow rate, Figure (2.7).
- for typical values of system parameters, the dynamic stability limit is to the left of, but close to, the peak of the compressor speed line. A good approximation is to use $\mathbf{P}_{C,m} < 0$ as the stability criterion.
- the static stability limit is only determined by the slopes of the compressor and the discharge valve characteristics, whereas the dynamic stability limit depends additionally on the ratio of inertia to capacitance in the system, L_u/V_p . The dynamic stability limit moves further to the left as this ratio is increased.
- non-dimensionalizing the pressure difference as $(\Delta p/\rho(\omega r)^2)$, and the mass flow rate as $(\dot{m}/\rho(\omega r)A_u)$, yields a system of equations primarily controlled by Greitzer's B -parameter defined as,

$$B = \frac{\omega r}{2 a} \sqrt{\frac{V_p}{A_u L_u}} = \frac{\omega r}{2 \omega_H L_u}, \quad (2.39)$$

where ω_H is the Helmholtz resonator natural frequency. The B -parameter can be given different physical interpretations, one of which is the ratio of compliance to inertia in the system. Therefore, it influences the system's dynamic stability limit. The significance of this parameter extends to the non-linear analysis where it controls the mode of instability as surge or rotating stall [10, 11].

- the system operating map, Figure (2.7), can be divided into three regions in terms of stability: the negatively sloped part of the compressor speed line where the system is always stable (e.g. point A), the positively sloped part of the compressor speed line (yet less positive than the valve slope) where the dynamic stability is set by the L_u/V_p ratio (e.g. point B), and the positively sloped part of the compressor (more positive than the valve slope) where the static stability criterion is violated and the system is unstable regardless of the L_u/V_p ratio (e.g. point C).

Case 2: Negligible Fluid Inertia

In this case, the inertia and compliance elements are the rotor and the plenum respectively. This simple second order model includes the driver and rotor inertia dynamics and thus emphasizes their role in the overall system dynamics.

The mathematical representation is obtained by setting the length of the compressor inlet duct, L_u , to zero in equation (2.29) as follows,

$$L_u \frac{d\dot{m}_C}{dt} = A_u \left(\Delta p_C(\dot{m}_C, \omega) - \Delta p \right) = 0, \quad (2.40)$$

The resulting non-linear algebraic equation states that $\Delta p_C(\dot{m}_C, \omega) = \Delta p$, which may be solved for \dot{m}_C provided that the compressor operation is limited to regions where the pressure rise–mass flow rate characteristic function, equation (2.6), is invertable,

$$\dot{m}_C = \dot{m}_C(\Delta p, \omega) = \rho \omega r A_u \Psi_C^{-1} \left(\frac{\Delta p}{\rho \omega^2 r^2} \right), \quad (2.41)$$

The system equations can then be written as,

$$\frac{d\omega}{dt} = \frac{1}{J} \left[\tau_T(\omega) - \tau_C(\Delta p, \omega) \right], \quad (2.42)$$

$$\frac{d(\Delta p)}{dt} = \frac{a^2}{V_p} \left[\dot{m}_C(\Delta p, \omega) - \dot{m}_V(\Delta p) \right]. \quad (2.43)$$

Since the inverse of the full compressor map is not single valued, Figure (2.4), it follows that the validity of this model is constrained to the neighborhood of some operating point around which this condition is satisfied. Therefore, the system described by equations (2.42) and (2.43) can not be used to simulate the non-linear surge behavior, nevertheless, it can be utilized to investigate the linear stability of a typical operating point.

Following the same linearization technique and notation used in the previous section, the linearized system equations are given by,

$$\frac{d}{dt} \begin{bmatrix} \tilde{\omega} \\ \Delta \tilde{p} \end{bmatrix} = \begin{bmatrix} \frac{1}{J} (\mathbf{T}_{T,\omega} - \mathbf{T}_{C,\omega}) & -\frac{1}{J} \mathbf{T}_{C,\Delta p} \\ \frac{a^2}{V_p} \mathbf{M}_{C,\omega} & \frac{a^2}{V_p} (\mathbf{M}_{C,\Delta p} - \mathbf{M}_{V,\Delta p}) \end{bmatrix} \begin{bmatrix} \tilde{\omega} \\ \Delta \tilde{p} \end{bmatrix}, \quad (2.44)$$

from which the characteristic equation can be found as,

$$\lambda^2 + \left[-\frac{1}{J}(\mathbf{T}_{T,\omega} - \mathbf{T}_{C,\omega}) - \frac{a^2}{V_p}(\mathbf{M}_{C,p} - \mathbf{M}_{V,p}) \right] \lambda + \frac{a^2}{JV_p} \left[(\mathbf{T}_{T,\omega} - \mathbf{T}_{C,\omega})(\mathbf{M}_{C,p} - \mathbf{M}_{V,p}) + \mathbf{M}_{C,\omega} \mathbf{T}_{C,p} \right] = 0. \quad (2.45)$$

The dynamic and static stability conditions translate to,

$$(\mathbf{T}_{C,\omega} - \mathbf{T}_{T,\omega}) > \frac{a^2 J}{V_p} (\mathbf{M}_{C,p} - \mathbf{M}_{V,p}), \quad (2.46)$$

$$(\mathbf{T}_{C,\omega} - \mathbf{T}_{T,\omega}) (\mathbf{M}_{C,p} - \mathbf{M}_{V,p}) < \mathbf{M}_{C,\omega} \mathbf{T}_{C,p}, \quad (2.47)$$

respectively. A comparison to case 1 leads to the following observation,

- the slopes $\mathbf{M}_{C,p}$ and $\mathbf{M}_{V,p}$ are equal to $1/\mathbf{P}_{C,m}$ and $1/\mathbf{P}_{V,m}$ respectively. These slopes were decisive to the stability in case 1.
- four additional slopes ($\mathbf{T}_{T,\omega}$, $\mathbf{T}_{C,\omega}$, $\mathbf{T}_{C,p}$ and $\mathbf{M}_{C,\omega}$) appear in case 2 due to the driver and rotor speed variations.
- similar to case 1, the static stability criterion depends only on the slopes of different characteristics whereas the dynamic stability criterion depends also on the ratio of inertia to compliance, J/V_p .
- Using typical values of these slopes, shows that the stable operation region can be extended to include a larger section of the positively sloped portion of the compressor speed line by reducing the value of J . This is due to the stabilizing effect of shaft dynamics which is discussed in the next section.

2.2.4 Physical Mechanism of Instability and Interpretation of Stability

Criteria

Discussion of Case 1

The physical mechanism of static instability can be understood by considering different steady state operating points on the map in Figure (2.7). For the negatively sloped part of the characteristics (e.g. point A), the pressure imbalance produced by perturbing the compressor mass flow rate will always act to restore the original operating point.

For instance, a small increase in the compressor flow causes the compressor pressure rise capability to decrease (according to slope of the speed line). The plenum, which provides the back pressure for the compressor, is at a higher pressure than what the compressor can deliver, and starts building up even more pressure due to the increased inlet mass flow from the compressor. The pressure imbalance between the plenum and the compressor discharge soon begins to decelerate the compressor flow, while the higher pressure transient in the plenum allows the discharge valve flow to increase, hence restoring the original plenum pressure and compressor flow. The system will always follow this behavior as long as the operating point is to the right of the peak and the perturbations are small enough for the linearized equations to hold. Note that the stability criteria, given by (2.37) and (2.38), are both satisfied in this part of the map regardless of the values of L_u , V_p and A_u .

In contrast, any flow disturbance (say increase) for an operating point located in the positively sloped part of the compressor speed line (yet less positive than the valve characteristic, point B for example) causes the compressor pressure rise to increase according to the positive slope. The plenum starts building up pressure

due to the increased inflow. The plenum pressure in this case always remains below that of the compressor discharge capability since the compressor follows its speed line instantaneously while the plenum lags behind due to its capacitive nature. This pressure imbalance keeps the compressor flow accelerating and more flow enters the plenum. Meanwhile the pressure difference across the discharge valve increases and so too does its flow. Note that because the valve slope is higher than the compressor, the flow through the valve is always less than the that through the compressor for a given plenum pressure, Figure (2.8)a.

The dynamic stability of such an operating point is determined by how rapidly these two actions (acceleration of the compressor flow and the pressure build up in the plenum) take place. The criticality of inertia to compliance ratio, L_u/V_p , to the stability in this part of the map can therefore be seen by considering two extreme cases. For a very large L_u/V_p , the small volume causes the plenum pressure to increase almost immediately as a response to an increase in mass inflow, the result of which is minimizing the pressure imbalance between the compressor and the plenum, hence minimizing the driving force that accelerates the compressor flow. The large inertia of the flow makes it even more difficult for the small pressure imbalance to produce significant acceleration. The discharge valve flow increases also as a response to the plenum increasing pressure, yet it remains less than the compressor flow (due to the more positive slope) and helps maintain the sufficient pressure in the plenum.

On the other hand, a very small L_u/V_p ratio causes the large volume plenum to respond very slowly to an increase in mass inflow. The plenum pressure, which remains almost constant, maximizes the aforementioned pressure imbalance, causing rapid accelerations of the compressor flow (small inertia) while minimizing

the effect on the discharge valve outflow. The result is that the system departs further from the original operating point.

Therefore, it can be shown that there is a critical value of L_u/V_p that sets the dynamic stability limit of the system at that operating point. The above scenarios can simply be verified by linear simulations of the system equations.

The third category of operating points that could exist is also on the positively sloped part of the compressor speed line but with a higher slope than that of the valve, Figure (2.8)b. In this case, the static stability criterion is violated. The physical mechanism of instability is independent of the inertia to compliance ratio. Considering an increase of the compressor flow produces a higher compressor pressure rise to causing the plenum pressure to rise. At this new pressure, the valve will discharge more flow out of the plenum than that supplied by the compressor (due to the difference in slope, Figure (2.8)b). The negative net inflow through the plenum tends to decrease its pressure, hence drawing more flow from the compressor and departing further from the original operating point. This sequence of events is only dependent on the slope of the compressor and discharge valve characteristics.

Discussion of Case 2:

In this case, similar arguments hold as far as the *initial* response of the compressor, plenum and discharge valve, to a small perturbation in mass flow rate is concerned. The main difference, however, is that as the compressor operating point starts to move along its pressure rise speed line, its torque changes and a torque imbalance across the rotor is produced. As a result, the rotor speed changes and the compressor moves to another speed line. The turbine operating point will also change, according to the change in rotor speed, by passing different amount

of flow and producing different torque. Therefore, depending on the shape (or local slope for linear analysis) of the compressor torque and pressure characteristic, the system response will either return to or depart from that operating point.

For example, starting from point A in Figure (2.9), an increase in compressor mass flow rate corresponds to a decrease in pressure rise across the compressor. It also corresponds to a decrease in its torque causing the rotor to start spinning up while the pressure imbalance between the plenum and the compressor is decelerating the compressor flow. The increase in rotor speed will soon reverse since the compressor will move to a higher torque speed line and the turbine will provide less torque. The final result is the restoration of the original operating point.

To understand the stabilizing effect of the shaft dynamics, consider an operating point to the left of the peak of the compressor pressure rise speed line, point B in Figure (2.9). An increase in compressor flow results in an increase in both its pressure rise and torque consumption. In this case the torque imbalance across the rotor will cause it slow down moving the compressor operating point to a lower speedline and thus to a lower pressure rise. Now the larger pressure imbalance between the plenum and the compressor discharge is more effective at decelerating the compressor flow and restoring the original operating point. It is important to notice that the rate at which these changes take place is of particular importance. A rotor with very small inertia will slow down rapidly (relative to the dynamics on the compressor side), hence moving the compressor to a lower pressure speed line and providing the maximum pressure imbalance needed to restore the original point. On the other hand, a very large rotor inertia tends to remain at the same speed while other transients take place.

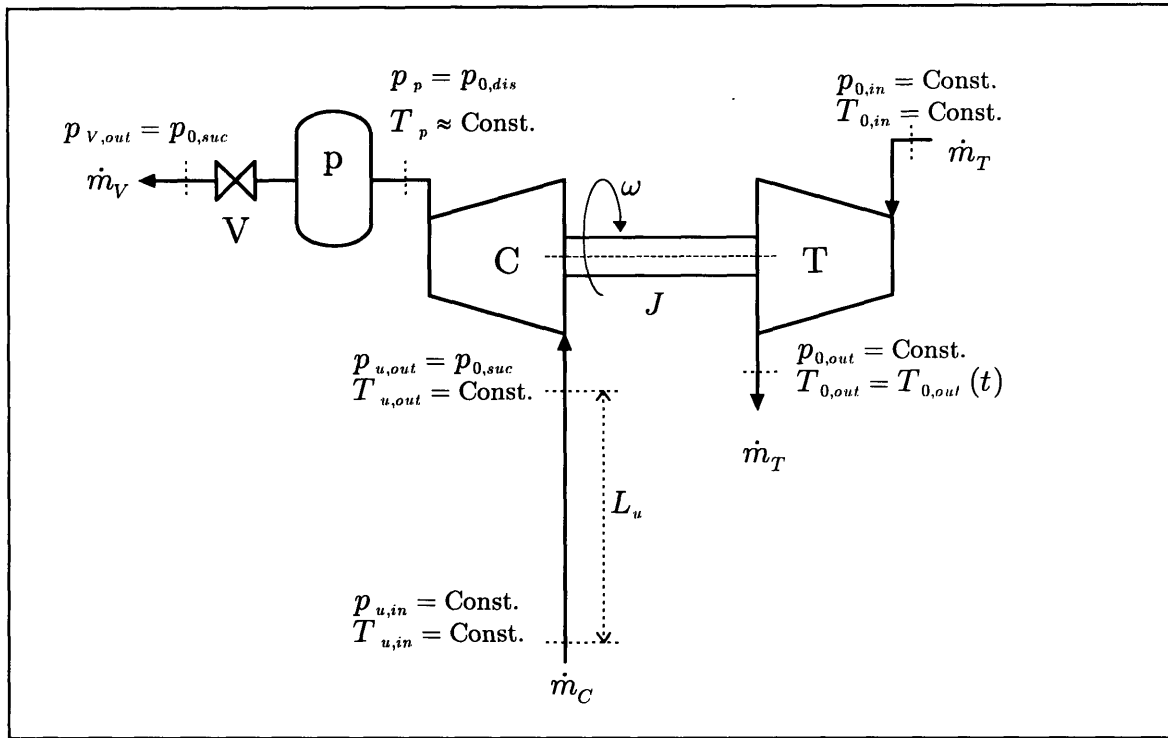


Figure (2.1) Schematic of the base-line pumping system

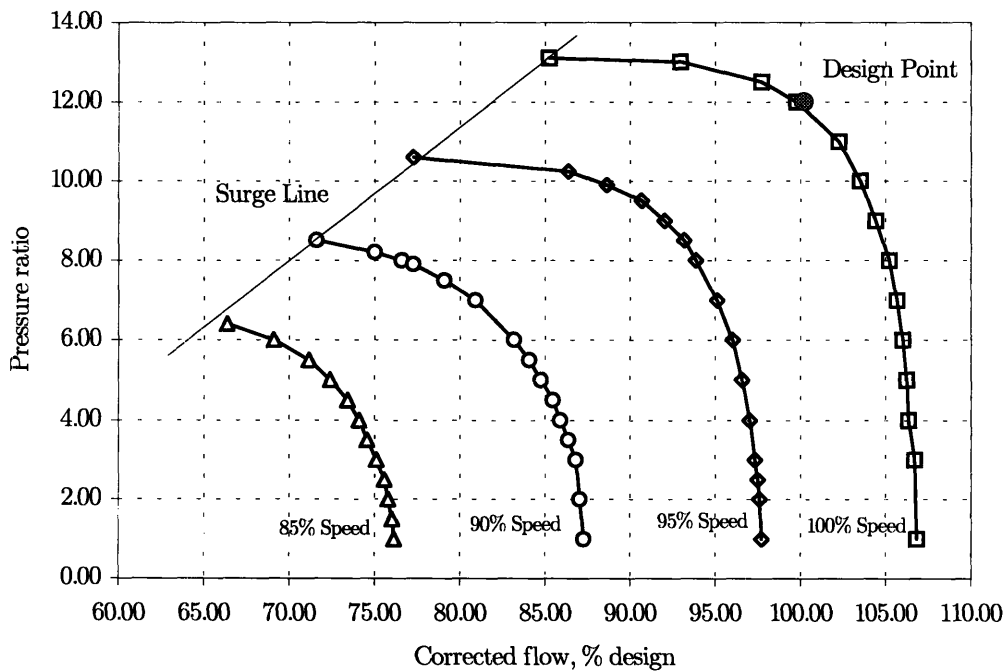


Figure (2.2) Typical compressor characteristics: pressure ratio versus mass flow rate for different operating speeds.

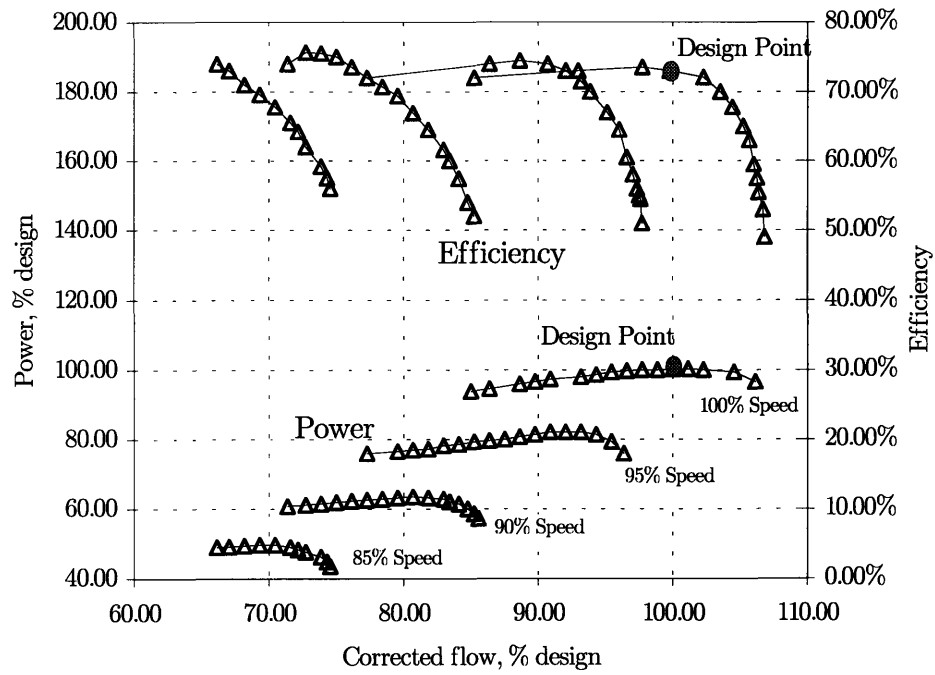


Figure (2.3) *Typical compressor characteristics: power and efficiency versus Mass Flow Rate for different operating speeds.*

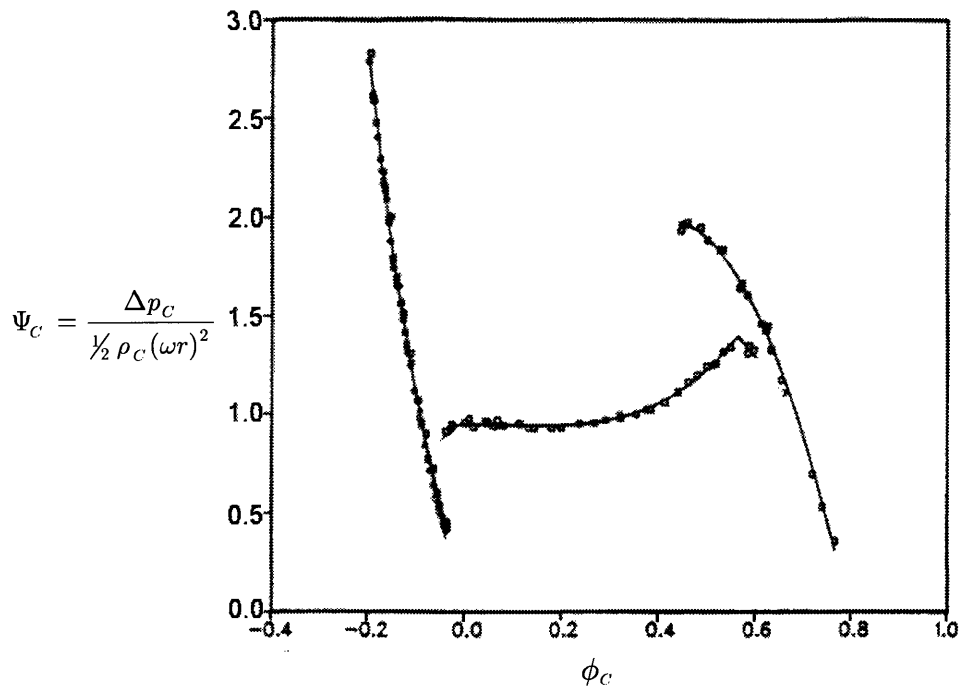


Figure (2.4) *Low pressure ratio compressor characteristics including the post-stall region, non-dimensionalized by rotor speed [8].*

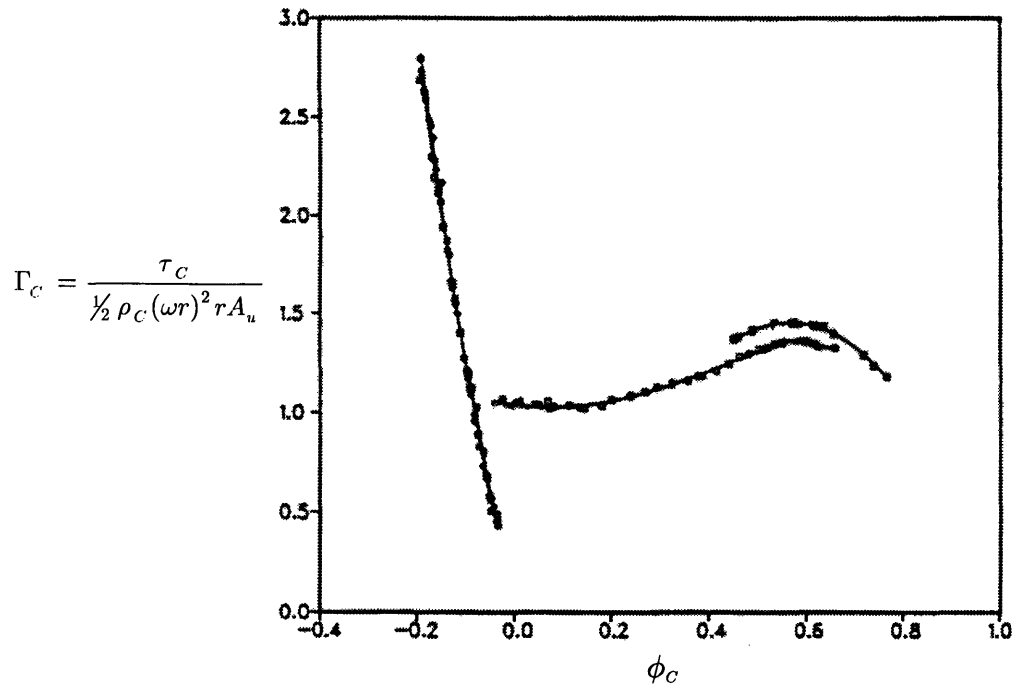
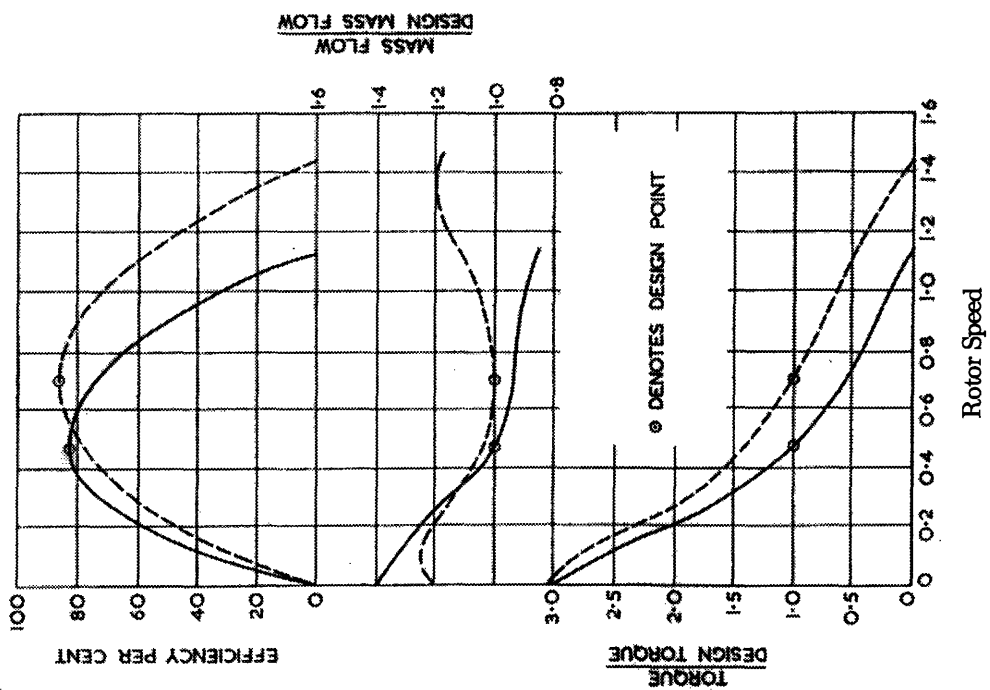
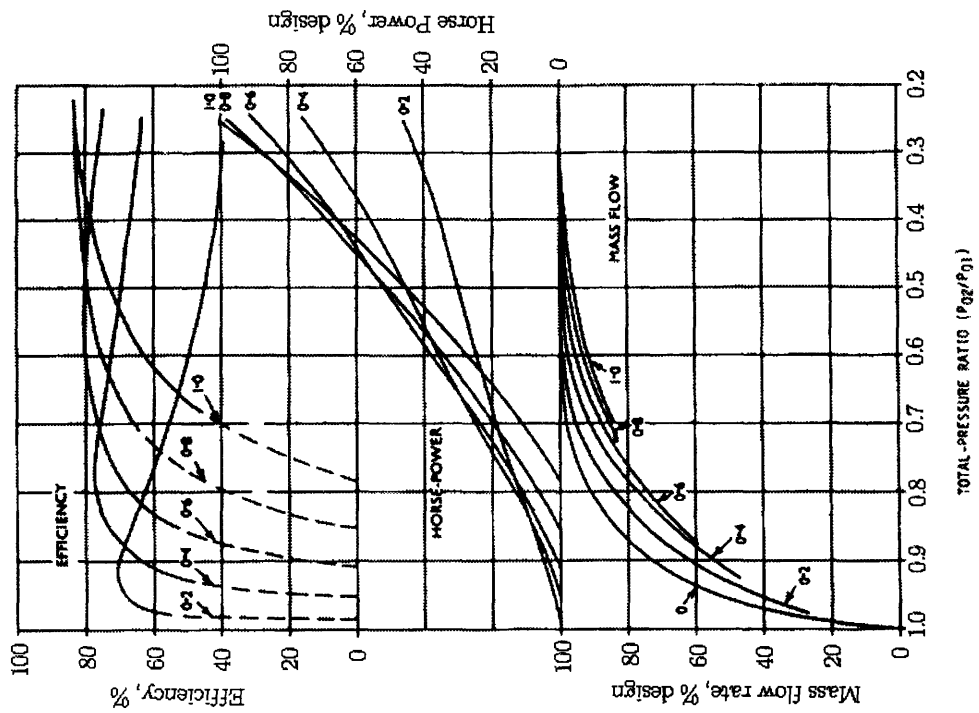


Figure (2.5) *Low pressure ratio compressor torque characteristics including the post-stall region, non-dimensionalized by rotor speed [8].*



(b)



(a)

Figure (2.6) Typical turbine characteristics: (a) mass flow rate, horsepower and efficiency versus pressure ratio for different operating speeds at a given inlet pressure [26]. (b) mass flow rate and torque versus rotor speed for a given pressure ratio [2].

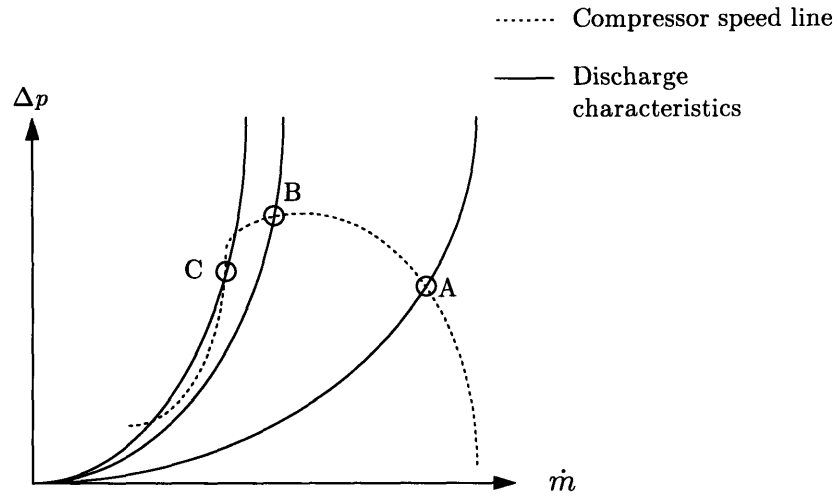


Figure (2.7) *System operating map: characteristics of compressor and discharge valve illustrating stability of different operating points.*

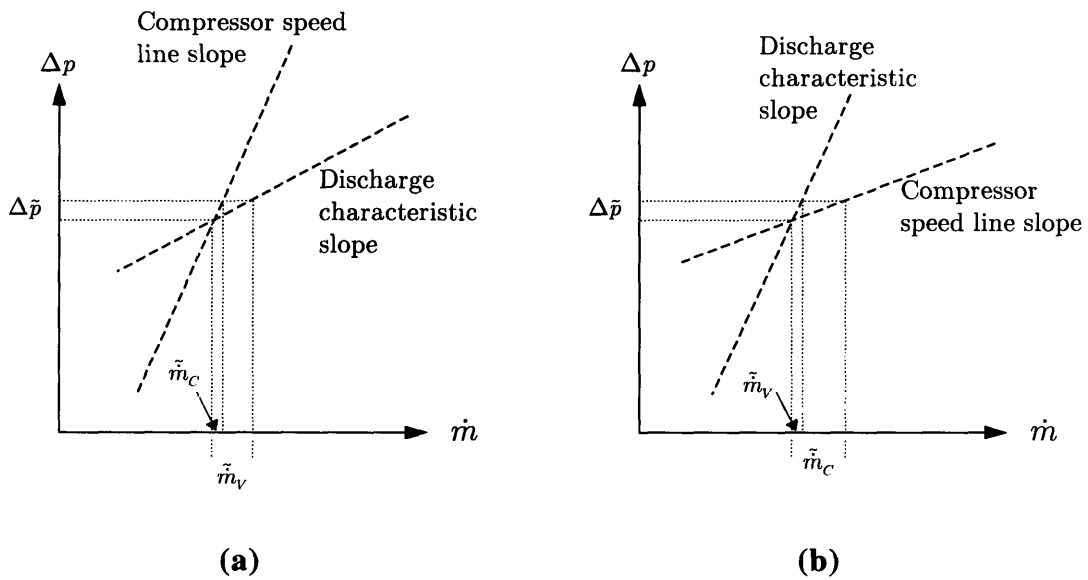


Figure (2.8) *Illustration of instability mechanisms.*

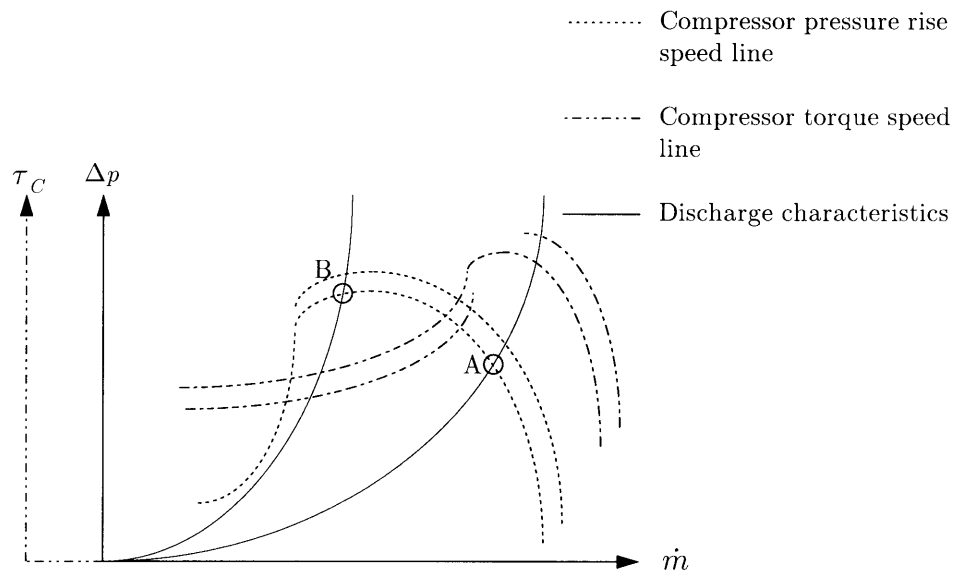


Figure (2.9) *Illustration of instability mechanism including rotor speed variations.*

Simulation and Analysis of a Basic Industrial Pumping System Model

This chapter presents a more elaborate analysis of the base-line model developed earlier. Specific mathematical forms of the turbine, compressor, and discharge valve constitutive relations are introduced. A simplified steady state analysis is performed to establish the steady state operating point. The resulting non-linear system of equations is numerically integrated under different kinds of disturbances and with different values of system inertia and compliance. The stability of the system at various operating points is also examined utilizing a linearized version of the equations. The validity of different modeling assumptions in the context of industrial pumping systems is also assessed.

The model is then augmented to include a turbine speed control system. The dynamics of the augmented model is examined by means of numerical simulations. Finally, general observations are assembled and discussed to explain the physics of the system and emphasize their practical significance.

3.1 Model without Turbine Speed Control

The considered system is represented by the model developed in the previous chapter as the base-line model, Figure (2.1). The same modeling assumptions described in section 2.2 still apply.

3.1.1 Formulation of Governing Equations

Turbine:

The turbine constitutive relation, given by equation (2.4) in a functional form, can be represented by the “ellipse law” which was first suggested by Stodola [24] as an empirical relationship, and was later given an analytical basis by Horlock [14]. A modified version of the ellipse law that accounts for rotor speed changes and that is consistent with the functional form of the turbine characteristics can be written as,

$$\frac{\dot{m}_T \sqrt{T_{0,in}}}{p_{0,in}} = e_1' \sqrt{1 - e_2' \frac{N}{\sqrt{T_{0,in}}} \left(\frac{1}{\pi_T} \right)^2}. \quad (3.1)$$

The turbine inlet temperature, $T_{0,in}$, is assumed to be constant throughout this study. The inlet pressure, however, is assumed constant only in the current case where no turbine speed regulation is considered. Thus, for generality purposes the turbine mass flow–pressure ratio relationship can be written as,

$$\dot{m}_T = p_{0,in} e_1 \sqrt{1 - e_2 \omega \left(\frac{1}{\pi_T} \right)^2}, \quad (3.2)$$

where e_1 and e_2 are constants specific to the turbine of consideration, and are to be determined based on actual steady state performance data.

The turbine torque characteristic is obtained from the steady state energy equation as,

$$\tau_T = \frac{\dot{m}_T C_{p,T} T_{0,in}}{\omega} \left[1 - \left(\frac{1}{\pi_T} \right)^{\frac{k-1}{k} \eta_T} \right]. \quad (3.3)$$

Initially, both the turbine efficiency and pressure ratio are assumed constant. Hence, the turbine mass flow and torque are function of rotor speed only. Figure (3.1) shows the turbine characteristics described by the above relationships. It can be seen, by comparison to typical data such as that in Figure (2.6), that these relationships capture part of the main trends of the turbine behavior.

In this model it is assumed that the turbine fluid is superheated steam at both inlet and exit. The thermodynamic properties are assumed to follow the ideal gas law for simplicity.

Compressor:

The compressor constitutive relation can be represented by two simple quadratic polynomials that cover the whole operating range including the post-stall region. Utilizing the non-dimensional forms presented by equations (2.5) and (2.17), the following polynomials can be introduced,

$$\Delta p_C(\dot{m}_C, \omega) = \rho_C(\omega r)^2 \begin{cases} c_1 + c_2 \phi_C'^2, & \phi_C' \leq \phi_{C,\text{critical}}' \\ c_3 \phi_C'^2 + c_4 \phi_C' + c_5, & \phi_C' \geq \phi_{C,\text{critical}}' \end{cases} \quad (3.4)$$

and,

$$\tau_C(\dot{m}_C, \omega) = \rho_C(\omega r)^2 r A_u \begin{cases} b_1 \phi_C' + b_2, & \phi_C' \leq 0 \\ b_3 \phi_C'^2 + b_4, & 0 \leq \phi_C' \leq \phi_{C,\text{peak}}' \\ b_5 \phi_C'^2 + b_6 \phi_C' + b_7, & \phi_C' \geq \phi_{C,\text{peak}}' \end{cases} \quad (3.5)$$

where, c_1, c_2, \dots, c_5 , and b_1, b_2, \dots, b_7 , are constant coefficients of the pressure rise and torque characteristics respectively. These coefficients can be calculated to match actual performance data of the machine considered in the study.

Figure (3.2) and Figure (3.3) show the compressor characteristics predicted by the above relationships in both dimensional and non-dimensional forms. Compar-

ing these characteristics to typical measured data such as those presented in Figure (2.4) and Figure (2.5), shows close agreement in terms of the values of the variables and slopes in different regions of operation. However, the typical data, shown in Figure (2.4) and Figure (2.5), of that particular compressor exhibit some additional features, such as hysteresis, not captured in this model.

Compressor Discharge Valve:

A simple non-linear form of resistive element constitutive relations is adopted here. The mass flow-pressure drop relation, expressed by equation (2.27) in functional form, can be given the form,

$$\dot{m}_V = \sqrt{(p_{V.in} - p_{V.out}) / k_V}, \quad (3.6)$$

and by assuming that $p_{V.out} = p_{u.in}$, and $p_{V.in} = p_p$, the discharge valve constitutive relation can be written as,

$$\dot{m}_V = \sqrt{\Delta p / k_V}. \quad (3.7)$$

Figure (3.4) shows the discharge valve characteristic described by the above equation.

Summary of Base-line model system equations:

The system dynamics are governed by the following set of non-linear ordinary differential equations,

$$\frac{d\omega}{dt} = \frac{1}{J} \left[\tau_T(\omega) - \tau_C(\dot{m}_C, \omega) \right], \quad (3.8)$$

$$\frac{d\dot{m}_C}{dt} = \frac{A_u}{L_u} \left[\Delta p_C(\dot{m}_C, \omega) - \Delta p \right], \quad (3.9)$$

$$\frac{d(\Delta p)}{dt} = \frac{a^2}{V_p} [\dot{m}_C - \dot{m}_V(\Delta p)], \quad (3.10)$$

where all the non-linear constitutive relations, namely τ_T , τ_C , Δp_C and \dot{m}_V , have been specified above.

3.1.2 Non-dimensionalization of Governing Equations

Following a typical non-dimensionalization procedure, similar to that adopted by Greitzer [10], yields an equivalent set of equations given by:

$$\frac{d\Omega}{d\tau} = 4\pi \frac{B^*}{J^*} [\rho^* \Gamma_T(\Omega) - \Gamma_C(\phi_C, \Omega)], \quad (3.11)$$

$$\frac{d\phi_C}{d\tau} = 4\pi B^* [\Psi_C(\phi_C, \Omega) - \psi_C], \quad (3.12)$$

$$\frac{d\psi_C}{d\tau} = \frac{\pi}{B^*} [\phi_C - \Phi_V(\psi_C)]. \quad (3.13)$$

Table (3.1) lists the main variables in the above equations and the reference quantities used for the non-dimensionalization, which results in the following characteristic parameters:

$$B^* = \frac{\omega_d r}{2a} \sqrt{\frac{V_p}{A_u L_u}} = \frac{\omega_d r}{2\omega_H L_u}, \quad (3.14)$$

$$J^* = \frac{J}{\bar{\rho}_C r^4 L_u}, \quad (3.15)$$

and,
$$\rho^* = \frac{\rho_{T,in}}{\bar{\rho}_C}. \quad (3.16)$$

Since the fluids in the turbine and the compressor are assumed to be the same through out, only the first two parameters remain of interest; namely B^* and J^* . B^* is essentially the same as Greitzer's B -parameter introduced earlier by equa-

tion (2.39), except that now it is based on the design point value of rotor speed. Similarly, in all other non-dimensionalizations involving rotor speed, the design point value has been used since the rotor speed it self is a state variable in this model.

B^* can be viewed as the ratio of effective fluid compliance to effective fluid inertia on the compressor side, while J^* can be viewed as the ratio of effective mechanical inertia to effective fluid inertia in the system. This non-dimensionalization has captured the similarity in the system and reduced the number of system physical parameters from three (J , L_u , and V_p), to two non-dimensional groups (B^* and J^*).

Quantity	Name	Reference Quantity	Non-dimensional Variable
ω	rotor speed	ω_d	Ω
\dot{m}_C	compressor mass flow rate	$\bar{\rho}_C \omega_d r A_u$	ϕ_C
Δp	system pressure rise	$\bar{\rho}_C (\omega_d r)^2$	ψ_C
t	time	$T_H = 2\pi / \omega_H$	τ
τ_C	compressor torque	$\bar{\rho}_C (\omega_d r)^2 r^3$	Γ_C
τ_T	Turbine torque	$\rho_{T,in} (\omega_d r)^2 r^3$	Γ_T
Δp_C	compressor pressure rise	$\bar{\rho}_C (\omega_d r)^2$	$\Psi_C(\phi_C, \Omega)$
\dot{m}_V	compressor discharge valve mass flow rate	$\bar{\rho}_C \omega_d r A_u$	$\Phi_V(\psi)$
k_V	compressor discharge valve coefficient	$k_{V,d}$	ζ_V

Table (3.1) *Base-line model non-dimensional variables and parameters*

In order to study the dynamics of the system, a steady state operating point (design point) must first be established to provide the mean point which a linearization process can be performed about, or to provide a suitable set of initial conditions for the numerical integration of the non-linear system. The steady state operating point is at the intersection of the compressor and the discharge valve characteristics, and when the compressor and turbine torques are balanced. To establish that point, a simple procedure is adopted in which part of the system variables and boundary conditions is specified based on typical industrial data, while the remaining part is calculated from component matching at equilibrium. Table (3.2) lists the values of critical system parameters resulting from such a procedure. Similarly, nominal values of system physical parameters, such as rotor inertia, plenum volume, etc., are selected based on typical industrial values. It should be noted however that industrial systems exist in numerous sizes. The choices made here are merely a representative example. Table (3.3) lists the nominal values of the system physical parameters both dimensional and non-dimensional.

Quantity	Value	Unit	Note
Turbine			
π_T	8.0	non-dim.	design choice
$T_{0,in}$	650.0	K	design choice (710 °F)
$T_{0,out}$	409.9	K	calculated from using π_T and η_T
\dot{m}_T	25.0	kg/sec	design choice, function of rotor speed
η_T	90%	non-dim.	design choice, initially constant
$P_T = P_C$	11.2407	MWatt	calculated (steady state matching)
$\tau_T = \tau_C$	14.051	kN.m	calculated (steady state matching)

Compressor			
ϕ_C	0.5	non-dim.	design choice
ψ	0.75	non-dim.	design choice
ω	800.0	rad/sec	design choice (≈ 7640 rpm)
$\bar{\rho}_C$	5.476	kg/m ³	average density of compressor flow. (calculated)
\dot{m}_C	93.67	kg/sec	calculated
Δp_C	0.657	MPa	calculated
π_C	2.46	non-dim.	calculated
Discharge valve:			
$p_{V.out}$	0.45	MPa	design choice (equal to $p_{u.in}$). Boundary condition
k_V	74.9	(kg.m) ⁻¹	calculated
\dot{m}_V	93.67	kg/sec	equal to \dot{m}_C at design point

Table (3.2) *Values of system variables and boundary conditions at design point.*

Parameter	Value	Unit	Note
J	200.0	kg.m ²	based on data given by [24]
r	0.5	m	assumed equal for both turbine and compressor
L_u	10.0	m	based on a relatively short upstream piping section
A_u	0.0855	m ²	based on 0.32 m pipe diameter (approx. 13")
V_v	50.00	m ³	based on approximate size of a process column
B^*	3.15	–	calculated, equation (3.14)
J^*	58.44	–	calculated, equation (3.15)

Table (3.3) *Values of system physical parameters*

3.1.3 Linear Stability Analysis

The linearized version of the system governing equations, given by equation (2.34), is now utilized to examine the stability of various operating points on the operat–

ing map as the two non-dimensional parameters B^* and J^* vary. For each value of the discharge valve coefficient, ζ_V , there exists at least one possible steady state operating point (fixed point) at which the two characteristics of the compressor and the valve intersect. The eigenvalues of the system's \mathbf{A} matrix, equation (2.34), are examined at each fixed point with different combinations of B^* and J^* values. The choice of ζ_V values is based on the analysis presented in section (2.2.3) where it was shown that the stability limit lies to the left of the compressor characteristics peak ($\zeta_{V,peak} = 1.7$ for the given compressor). Therefore, values of 1.72 to 2.3 were used for ζ_V , where B^* and J^* were varied between 10^{-4} and 10^3 , all for a single compressor speed line.

The results of this exercise are shown in Figure (3.5). In part (a) of the figure, the stability of one fixed point, namely $\zeta_V = 2.0$, is examined. The curve shown divides the plane into a stable and unstable range of B^* and J^* combinations. In part (b) of the figure, the stability of additional fixed points is shown. Each curve in the figure corresponds to a single value of ζ_V (i.e. one throttling position or one fixed point), and splits the plane into a stable and unstable regions—the stable part being always associated with the lower values of B^* and J^* . Considering, for example, the curve corresponding to $\zeta_V = 1.8$, it is found that for values of B^* less than 0.6 the fixed point is stable regardless of the value of J^* . However, for slightly higher values of B^* there exists a corresponding critical value for J^* below which the system is stable at that particular fixed point. Furthermore, for very high B^* stability of that fixed point becomes totally dependent on J^* alone.

Increasing the throttling setting, ζ_V , slightly further (up to 2.15), causes the stable region of B^* and J^* to shrink, while maintaining the same qualitative nature of the dependency between B^* and J^* in determining the stability. That

dependency changes once a critical value of ζ_V is reached. Any further throttling beyond that critical point starts to diminish the stabilizing effect of the driver dynamics. At a throttling setting of 2.3, the stability boundary becomes almost a horizontal line below which that fixed point is stable regardless of the value of J^* . This figure is used as a guide in selecting values for B^* and J^* to demonstrate both the stable and unstable transient behavior of the system.

3.1.4 Simulation of the Non-linear Model

The numerical integration of the system's governing equations (3.8–10 or 3.11–13) was carried out using the MATLAB computational environment and the appropriate toolboxes. In order to enhance the reliability of the numerical results, the simulations were carried out repeatedly with different time steps and integration routines. The results presented in this study showed no sensitivity to either of these factors.

The system's response to a step input in the compressor discharge valve set point is first examined by abruptly changing the value of ζ_V (increasing ζ_V represents closing the valve and moving the operating point to the left on the compressor map). The time at which the step occurs is generally at 20% of the total time of the simulation, and is indicated in the caption of each figure. In the following simulations, it is assumed that the system starts from a stable steady state operating point, at which the values of the states represent the initial conditions to the integration routine. Two examples are presented in Figure (3.6) and Figure (3.7). The first is a demonstration of the post-stall behavior achieved by throttling the discharge valve beyond the stability limit predicted by the linear analysis in the previous section. The response takes the form of sustained oscillations in all three states of the system with a period called the surge period. In

this simulation the nominal values of B^* and J^* were used (3.15 and 58.44 respectively). The second simulation shows the stabilizing effect of small values of B^* , specifically $B^* = 0.1$, where values of 5.0 and 58.44 were used for ζ_V and J^* respectively. The response took the form of a quick oscillatory transient that died out approaching a new *stable* operating condition on the positively sloped part of the compressor characteristics, which corresponds to a mode of compressor operation known as rotating stall. Rotating stall is captured by the current model only by means of the axisymmetric characteristics provided as an input, and although rotating stall is known to be an instability local to the compressor, this model presents it as a stable *system* operating condition. It is characterized by operating at reduced mean compressor flow and pressure rise. At such a condition the internal compressor flow field is unstable, however, the system does not have enough compliance (i.e. B^* is small) to sustain surge oscillations.

The effect of B^* and J^* on the post-stall behavior of the system is examined through a series of simulations with parameter values selected from Figure (3.5) such that a system instability (surge) occurs. The simulations start by perturbing the system (small offset in initial conditions) from an unstable fixed point at $\zeta_V = 2.1$. B^* is varied from 1 to 20 and J^* is varied from 1 to 1000. The results are summarized in Figure (3.8). It can be seen from the figure that B^* has a dominant effect on the surge period confirming that the instability is an interaction between the fluid compliance and fluid inertia (captured in B^*) on the compressor side. It can also be seen that at high values of B^* , decreasing J^* has the effect of increasing the surge period. That can be explained by recalling that small values of J^* have a stabilizing effect which causes the surge cycles to be further apart.

3.2 Assessment of Model Assumptions

3.2.1 Effect of Driver Efficiency Variations

In the formulation above, it was assumed that the turbine efficiency is constant. However, during a transient the turbine mass flow rate, torque supply and efficiency are expected to change. The changes of mass flow rate are captured by the turbine constitutive relation given by equation (3.2). Turbine torque is obtained by applying a simple control volume energy balance for the turbine, and is found to depend on the turbine mass flow, pressure drop and efficiency, as can be seen from equation (3.3). Thus, the assumption of constant efficiency plays a role in determining the torque supply from the turbine. Furthermore, the rotor inertia acceleration is controlled by the balance of compressor and turbine torques. Since it was established that the turbine pressure ratio is constant, the efficiency is only a function of rotor speed (section 2.2.2). Figure (2.6) shows a typical variation of turbine efficiency with rotor speed for a given pressure ratio. Such a trend can simply be captured using a single quadratic polynomial as follows,

$$\eta_T(\omega) = f_1(\omega - f_2)^2 + f_3, \quad (3.17)$$

where f_1 , f_2 , and f_3 are constant. Assuming that the turbine best efficiency point is at the design point, and realizing that the turbine efficiency is zero at zero speed and at no load speed (runaway speed) these constants can be found as:

$$f_1 = -(f_3/f_2), \quad f_2 = \eta_{T,max}, \quad f_3 = \omega_d.$$

Figure (3.9) shows the resulting efficiency, mass flow and torque as a function of rotor speed. Comparing the torque variation in this case to that used in the simulations above, and shown in Figure (3.1), shows that for rotor speed values between 60% and 200% of design speed, introducing efficiency variations does not

have much effect on estimating the torque. For rotor speeds below 60% of design, the constant efficiency assumption results in overestimating the turbine torque by almost a factor of 2.

The impact on dynamics can be assessed by examining the maximum fluctuations in rotor speed during a transient. In the above simulations, maximum speed fluctuations occurred during surge cycles with small values of J^* . In all cases the minimum speed was always above 60% of design speed. Thus introducing efficiency variations would not make any significant effect.

However, when considering large transients involving reduced rotor speeds, the efficiency variation would be a more suitable choice. Examples of such transients are system shut-down, system start up, and the recovery from surge using a re-cycle line.

3.2.2 Effect of Compressor Pressure-Rise Time Lag

The assumption examined here is the quasi-steady behavior of the compressor. Data show that in certain ranges of the compressor operating map, the compressor pressure rise does not respond instantaneously to changes in mass flow rate. Instead, it lags behind in a manner similar to that of a first order system response. To capture this effect, a first order time lag is introduced to link the quasi-steady pressure rise that follows the compressor characteristics, and the actual lagging pressure rise. Mathematically, this can be stated as,

$$\tau_{lag} \frac{d(\Delta p_{C,inst})}{dt} = \Delta p_C - \Delta p_{C,inst}, \quad (3.18)$$

where,

$$\tau_{lag} = \begin{cases} \tau_{lag} & 0 < \phi'_C < \phi'_{C,peak} \text{ and } \frac{d\dot{m}_C}{dt} < 0 \\ 0 & \text{elsewhere} \end{cases} \quad (3.19)$$

and $\Delta p_{C,inst}$ is the compressor instantaneous pressure rise. This formulation was first introduced by Greitzer [10]. He concluded from available data and from numerical simulations that the dynamics of the basic compression system considered in his study has a weak effect on the overall system dynamics. Similar findings were concluded using the base-line model together with equation (3.18), where simulations with and without this effect came out almost identical. This is due to the fact that the time lag constant is a property of the compressor and is usually proportional to a certain number of rotor revolutions needed to develop the stall cell in the compressor. This number of rotor revolutions is roughly the same for a wide class of compressors. In addition, this time lag is in effect only in a limited region of the compressor map, as indicated by equation (3.19), where the compressor operating point is moving towards the stall line. In other regions of operation, data show that the compressor pressure rise adheres closely to its quasi-steady characteristics. Nevertheless, the inclusion of this effect has a minor stabilizing effect. That can be explained by recalling (from section 2.2.4) that the stability limit to the left of the characteristics peak is affected by the amount of pressure imbalance between compressor discharge and the plenum. A compressor with a pressure rise time lag would produce lower discharge pressure than that of a quasi-steady compressor at any given time during the transient. Thus, the pressure rise time lag results in a less positive effective characteristics slope, Figure (2.8)a.

Although the value of the time lag constant could be obtained from experiment for existing machines, it is useful to know that current CFD models of the compressor internal flow can explain and quantify such a phenomena.

3.3 Model with Turbine Speed Control

The driver in an industrial pumping system is always equipped with a speed control device to maintain constant speed during regular operations and to provide a means of changing the system operating point upon demand. For a steam turbine, this device consists of a speed sensor, a controller, an actuation mechanism, and a throttle valve at the inlet of the turbine. The controller usually uses a PID control law. The actuation mechanism is a network of hydraulic and mechanical elements that amplifies the controller output and communicates it to the throttle valve¹.

3.3.1 Formulation of the Speed Governor Control

The governor mechanism and the throttle valve are modeled as a lumped stiffness, damping and inertia.

Figure (3.10) shows a schematic of the system including the turbine speed control sub-system. The base-line model, represented by equations (3.8–10 or 3.11–13), is augmented in the following manner.

Turbine Inlet Throttle Valve:

The flow across this valve is assumed incompressible (low Mach number). A simple quadratic function is used to represent its constitutive relation,

$$\dot{m}_t = \sqrt{(p_{t,in} - p_{0,in}) / k_t}, \quad (3.20)$$

where, $p_{t,in}$ is the total pressure at the valve inlet, and is considered as a constant boundary condition. k_t is the valve throttling coefficient for which higher values

¹ Detailed design description of these subsystems is available in [22, 24] amongst others.

are associated with the closure of the valve. It should be noted that $p_{0,in}$, the turbine inlet total pressure, is no longer constant. Instead, it varies at different throttling settings and turbine speeds such that the mass continuity between the valve and the turbine is satisfied. Therefore, the value of $p_{0,in}$ can be evaluated algebraically by equating the right hand sides of equation (3.2) and (3.20) and solving for $p_{0,in}$. The result can be written in terms of $\pi_T = (p_{0,in}/p_{0,out})$ and $\pi_t = (p_{t,in}/p_{0,out})$ as follows,

$$\pi_T = \frac{-1 + \sqrt{1 + 4 e_1^2 k_t p_{0,out} (e_1^2 e_2 k_t p_{0,out} + \pi_t)}}{2 e_1^2 k_t p_{0,out}} \quad (3.21)$$

Consequently, the turbine constitutive relations are now functions of both rotor speed and pressure ratio, since the turbine pressure ratio is no longer constant. Another assumption is that the temperature remains constant across the valve, consistent with the general assumptions of a throttling process.

The last relation needed to complete the model of the throttle valve is one that links the throttle valve coefficient, k_t , to the position of the valve gate, x_t . Such a relation would be required to give infinite value of k_t at the fully closed position of the valve (corresponding to a maximum value of x_t), while giving a finite value of k_t at the fully opened valve position (corresponding to a minimum value of x_t). A possible choice is an exponential function of the form,

$$k_t = z_1 e^{z_2 x_t}, \quad (3.22)$$

where z_1 and z_2 are constants.

Governor Control Law:

A basic PID controller can be described by,

$$F_G(t) = K_p \left(E + T_D \frac{dE}{dt} + \frac{1}{T_I} \int_{t_0}^t E dt \right), \quad (3.23)$$

where, F_G is the output force signal, $E = (\omega - \omega_{ref})$ is the input error signal, and K_p , T_D and T_I are controller constants to be selected.

Governor Mechanism and Valve Dynamics:

The governor mechanism and throttle valve (referred to as the mechanism) are lumped into a mass-spring-damper system, with the governor output, F_G , as external forcing,

$$m_G(\ddot{x}_t + 2\zeta_G \omega_{n,G} \dot{x}_t + \omega_{n,G}^2 x_t) = F_G(t), \quad (3.24)$$

where m_G is the equivalent mass of the mechanism, x_t is the position of the throttle valve, ζ_G is the effective damping ratio, and $\omega_{n,G}$ is the undamped natural frequency of the mechanism.

In order to incorporate the above equations into the model, they have to be written in state space form. This can be achieved by writing the above two equations in transfer function form. Simple manipulations can then yield an equivalent set of equations that is easily transformed into state space format. Briefly, this can be written as,

$$\begin{aligned} \frac{X_t(s)}{E(s)} &= \frac{X_t(s)}{F_G(s)} \frac{F_G(s)}{E(s)} \\ &= \left(\frac{1}{m_G(s^2 + 2\zeta_G \omega_{n,G} s + \omega_{n,G}^2)} \right) \left(-K_p \left[1 + T_D s + \frac{1}{T_I s} \right] \right), \end{aligned} \quad (3.25)$$

which is equivalent to,

$$\begin{aligned} \frac{X_t(s)}{E(s)} &= \frac{X_t(s)}{\xi(s)} \frac{\xi(s)}{E(s)} \\ &= \left(1 + T_D s + \frac{1}{T_I s} \right) \left(\frac{-K_p}{m_G(s^2 + 2\zeta_G \omega_{n,G} s + \omega_{n,G}^2)} \right), \end{aligned} \quad (3.26)$$

where ξ is an intermediate variable. Transforming the two transfer functions in the above equation back to the time domain results in the following state equations,

$$\dot{y}_1 = y_2, \quad (3.27)$$

$$\dot{y}_2 = -\frac{K_p}{m_G}(\omega - \omega_{ref}) - 2\zeta_G \omega_{n,G} y_2 - \omega_{n,G}^2 y_1, \quad (3.28)$$

$$\dot{y}_3 = y_1, \quad (3.29)$$

and the output equation is given by,

$$x_t = x_{t,d} - (y_1 + T_D y_2 + \frac{1}{T_I} y_3). \quad (3.30)$$

Where the three states are defined as,

$$y_1 = \xi, \quad y_2 = \dot{\xi}, \quad \text{and} \quad y_3 = \int \xi dt.$$

Summary of System Model with Driver Speed Control:

The system dynamics is now described by six state equations, constitutive equations of all components, mass continuity for the turbine, and an output equation:

$$\text{State Equations} \quad \frac{d\omega}{dt} = \frac{1}{J} \left[\tau_T(\omega) - \tau_C(\dot{m}_C, \omega) \right], \quad (3.31)$$

$$\frac{d\dot{m}_C}{dt} = \frac{A_u}{L_u} \left[\Delta p_C(\dot{m}_C, \omega) - \Delta p \right], \quad (3.32)$$

$$\frac{d(\Delta p)}{dt} = \frac{a^2}{V_p} [\dot{m}_C - \dot{m}_V(\Delta p)], \quad (3.33)$$

$$\dot{y}_1 = y_2, \quad (3.34)$$

$$\dot{y}_2 = - \frac{K_p}{m_G} (\omega - \omega_{ref}) - 2 \zeta_G \omega_{n,G} y_2 - \omega_{n,G}^2 y_1, \quad (3.35)$$

$$\dot{y}_3 = y_1, \quad (3.36)$$

The output equation, (3.30), is used to calculate the turbine throttle position, from which the throttling coefficient, k_t , can be found using equation (3.22). The constitutive relation pertaining the turbine throttle valve, equation (3.20), in conjunction with the mass continuity between the throttle and the turbine, equation (3.21), are also used to determine the turbine mass flow and pressure ratio, both of which are needed to calculate the turbine torque.

Selection of Model Parameters:

The introduction of the turbine speed governor into the model produced many parameters for which a value needs to be selected. Table (3.4) lists the main parameters, the selected values and the basis of selection.

Parameter	Description	Value	Note
K_P	controller gain	6.2	Estimated using Ziegler–Nichols rules for tuning PID's, [18].
T_D	derivative control time constant	0.6	
T_I	integral control time constant	2.4	
m_G	equivalent mass of throttling mechanism	100 kg	Design choice
ζ_G	equivalent damping	0.5	Design choice (underdamped)

	ratio		
$\omega_{n,G}$	equivalent natural frequency	10 rad/sec	Design choice
z_1	throttle valve constant	0.19	selected such that reasonable throttling is obtained
z_2	throttle valve constant	29.9	selected such that reasonable throttling is obtained

Table (3.4) *Nominal values of turbine governor sub-system parameters.*

3.3.2 Analysis of the System Model with Speed Control

The model presented above allows the effect of the turbine speed control on the overall system dynamics to be examined. In particular, the post-stall behavior and transients involving large shifts in system operating point can be investigated.

Numerical simulations of the above model show that the turbine speed control does not have an appreciable effect on post stall behavior. The only pronounced effect can be seen in the amplitude of oscillations in rotor speed during surge with small values of J^* and reasonably large values of the controller gain, K_p . Figure (3.11) and Figure (3.12) show two simulations demonstrating the post-stall behavior of the system without and with speed control respectively, both using involve the response to a step input in $\zeta_V = 1.0$ to 2.5, and values of $B^* = 3.15$ and $J^* = 0.3$. Comparing the two simulations yields the following observations. The oscillations in rotor speed have higher amplitude with no speed control as compared to the case with speed control (about 40% higher). The reason for that is the corrective action that the controller takes responding to the speed fluctuations associated with the surge cycle. The small value of J^* makes it possible for the rotor inertia to accelerate and decelerate on the same time scale of the surge oscillation. It can

also be observed that the surge period is slightly shorter and that the system instability developed earlier in the case having speed control. All three observations lead to the conclusion that the effect of speed control on the system post-stall dynamics can be thought of as a higher effective J^* , since it reduces the amplitude of speed oscillations, slightly shortens the surge period, and diminishes the stabilizing effect of small values of J^* .

Transients of finite amplitude can be encountered when the system operating point is intentionally changed for operational reasons. A typical example is the process of shutting down the pumping system. The speed control system is the main device used to achieve such an action.

To examine the dynamics associated with these transients, consider the case where the system is at a typical steady operating point. The reference speed, ω_{ref} , is set to zero and the system response is then observed. The trajectory of the system response on a phase plane (such as the compressor map) was found to depend strongly on B^* , J^* , and driver speed control parameters. In particular, it was found that increasing the value of K_p above a critical value can cause the system to experience a surge cycle during a shut-down transient. A very high value of K_p corresponds to a large control signal that closes the throttle valve immediately. Consequently, the turbine mass flow, and hence the torque, drops to zero, and the rotor inertia is left to decelerate under the action of the compressor torque alone, which in turn depends on the instantaneous shaft speed and compressor flow. This chain of dependency can be best understood by means of two simulation examples: one with high K_p (causing surge), and one with low K_p (avoiding surge). Figure (3.13) and Figure (3.14) show the results of these simulations. In Figure (3.13), the high value of K_p resulted in the immediate loss of the turbine torque.

The values of B^* and J^* used in the simulation correspond to a slow plenum discharge rate (relative to the deceleration of the rotor) that maintained a high back pressure on the compressor long enough to reduce the flow rate below the stability threshold at that speed. In contrast, the simulation with small K_p , Figure (3.14), shows that the throttle valve closure was slow enough for the dynamics on the compressor side to catch up. The result is a transient trajectory that closely follows the compressor discharge valve line, tracing all the possible steady operating points at different speeds.

3.4 Discussion of Results

In this section, a summary of the observations made above is presented. Practical issues regarding the formulation of the model and the implications of the results are discussed.

The third order model of the base-line system was able to capture a wide spectrum of dynamics of interest. The two non-dimensional groups, B^* and J^* , were shown to have a significant impact on the stability of the system and an appreciable role in the post stall behavior of the system. It should be noted that for a real industrial installation, obtaining accurate estimates of these parameters could be nontrivial. In building the model for a practical system, care should be taken in identifying the *effective* fluid compliance, fluid inertia and mechanical inertia, which are not necessarily obtained from the physical dimensions of the corresponding elements. System identification tests may be utilized for a given system to obtain more accurate estimates of the *effective* values of these parameters. For example, a discharge valve might not be the only component responsible for throttling the compressor—the internal construction of a process

column (plenum) can have a significant throttling role. The presence of a check valve at the compressor discharge can play a similar role. Another example is identifying the effective compressor duct inertia. A reasonable choice for the inlet piping section can be identified as that between the compressor and the closest upstream plenum², provided this plenum is large enough to have a much slower dynamics than the system of consideration.

The parameters of the lumped model introduced for the governor/throttle mechanism can also be determined using system identification tests, since there is usually no single mass, spring or damper that can represent the dynamics of the overall mechanism.

The results obtained from analyzing this model indicated that smaller values of J^* , defined by equation (3.15), have a stabilizing effect up to a certain compressor throttling level. Reducing J^* can be achieved by either reducing the rotor inertia or increasing the compressor inlet duct fluid inertia. For the designer of such systems that indicates the use of shorter and lighter rotor shafts with smaller diameters. Additionally, the location of the compressor upstream plenum mentioned above can be selected to be as far as possible from the compressor in order to further reduce J^* . It should be understood, however, that many other design considerations have to be accounted for in making such design choices. Similarly, smaller values of B^* , defined by equation (3.14), were shown to have a stronger stabilizing effect. Comments parallel to those made for J^* can be argued for B^* from a design point of view.

² In actual installations, there is usually a plenum upstream the compressor that is used to mix the recycled and fresh gas before entering the compressor in order to remove any condensate and to provide some cooling for the recycled gas.

The role of governor controller parameters in any problematic situation can be examined and explained using the model. The observation that higher controller gain tends to diminish the stabilizing effect of small J^* can assist the designer in evaluating different design choices regarding the controller parameters. The model can also be utilized in estimating the maximum controller gain allowable for a shut down action to be surge-proof for a given system.

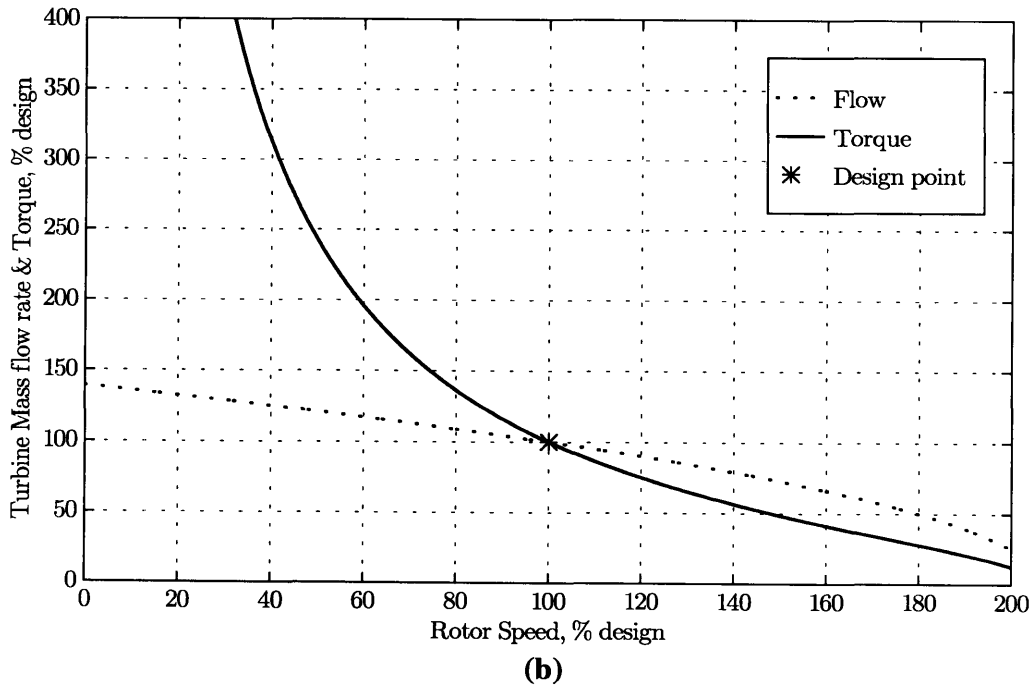
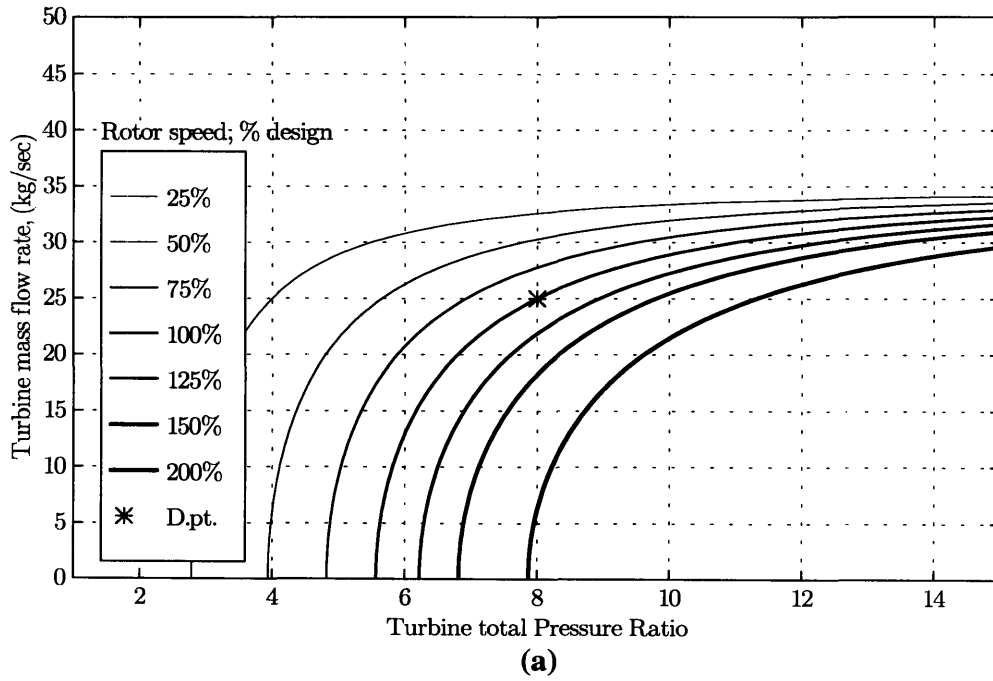


Figure (3.1) *Turbine characteristics: (a) mass flow rate-pressure ratio. (b) flow and torque as function of rotor speed. Both for a given turbine inlet pressure.*

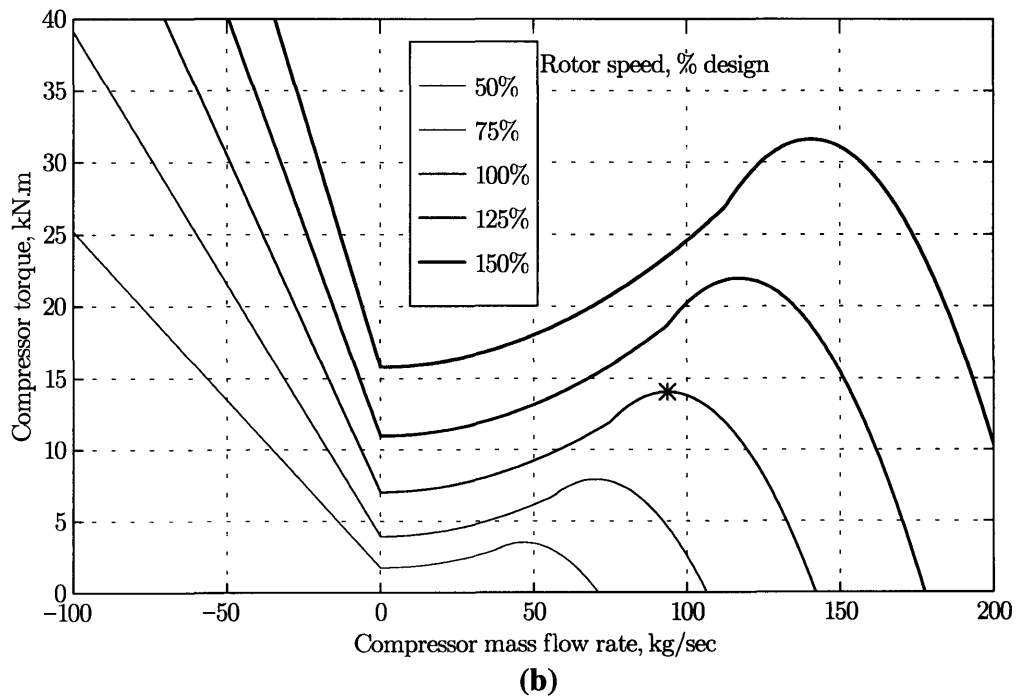
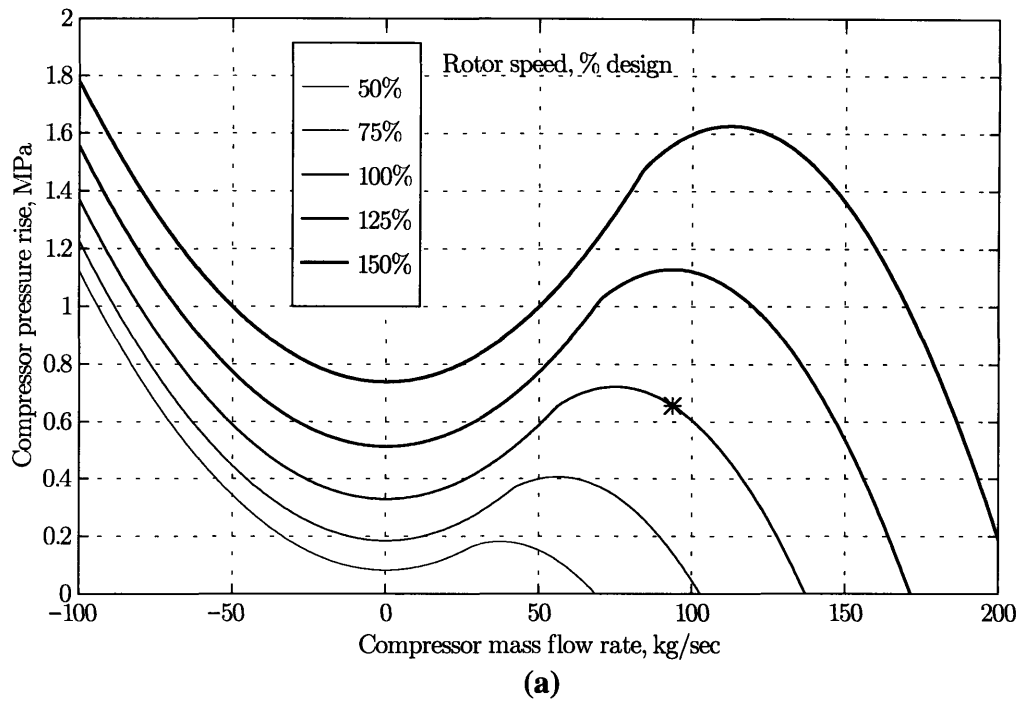


Figure (3.2) Compressor characteristics: (a) pressure rise-mass flow rate. (b) torque-mass flow rate. Both in dimensional form showing different speed lines.

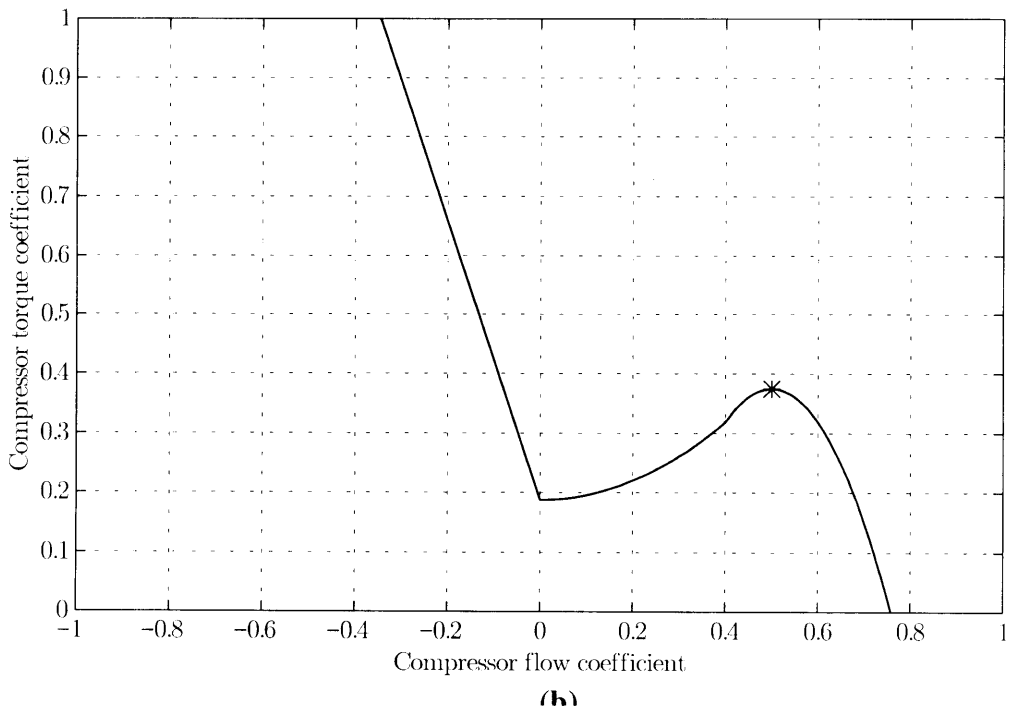
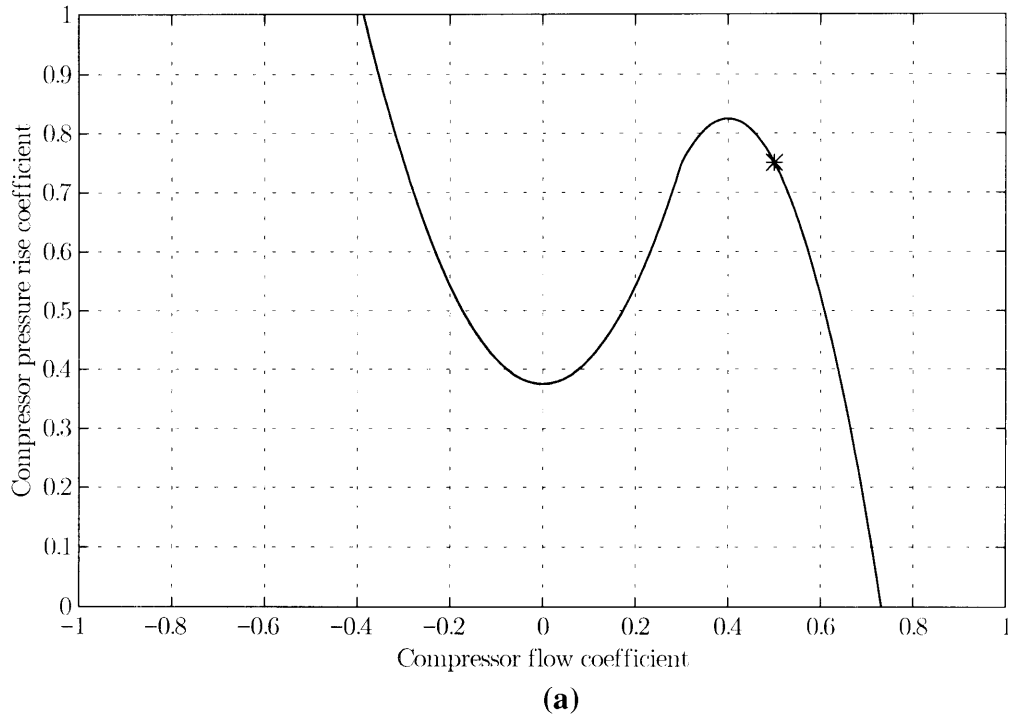


Figure (3.3) *Non-dimensional compressor characteristics: (a) pressure rise coefficient-flow coefficient. (b) torque coefficient-flow coefficient. (eq. 2.16, 17)*

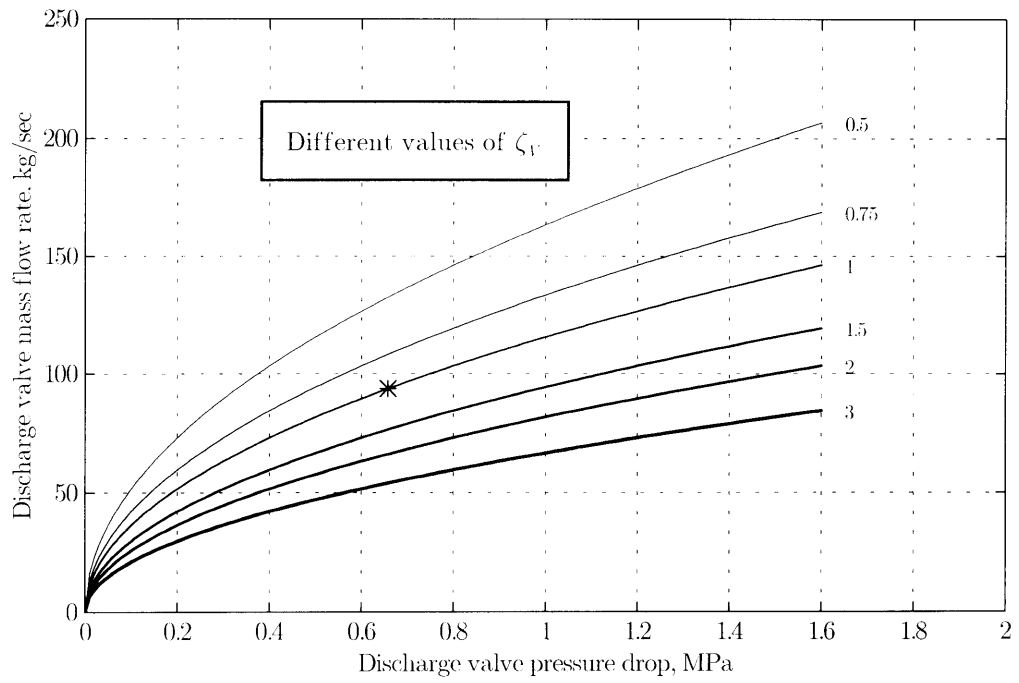


Figure (3.4) *Discharge valve characteristics: mass flow rate-pressure rise, for different values of ζ_v .*

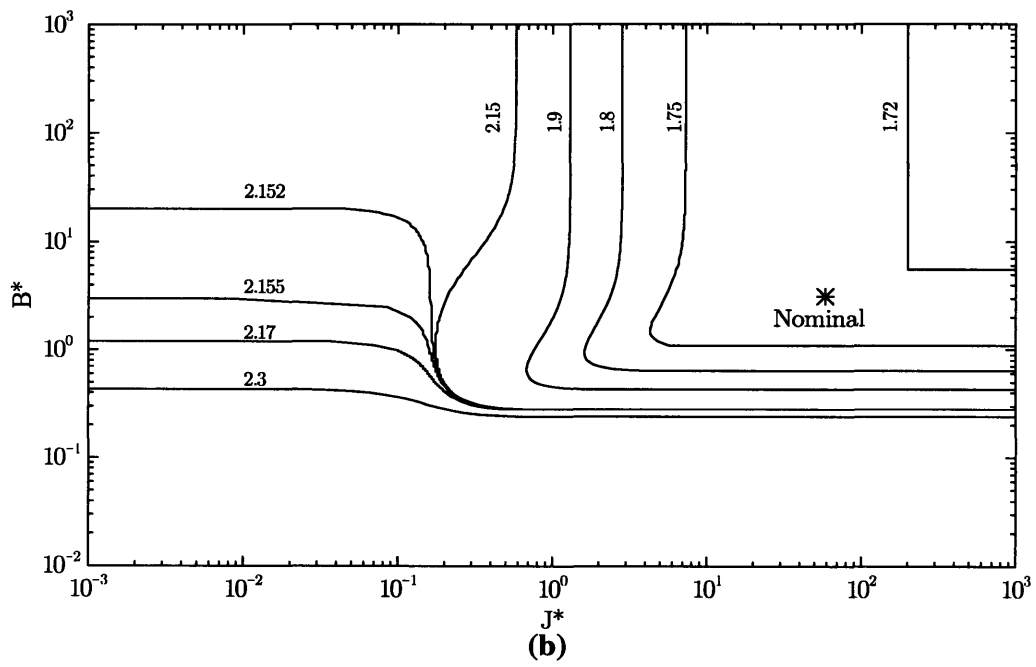
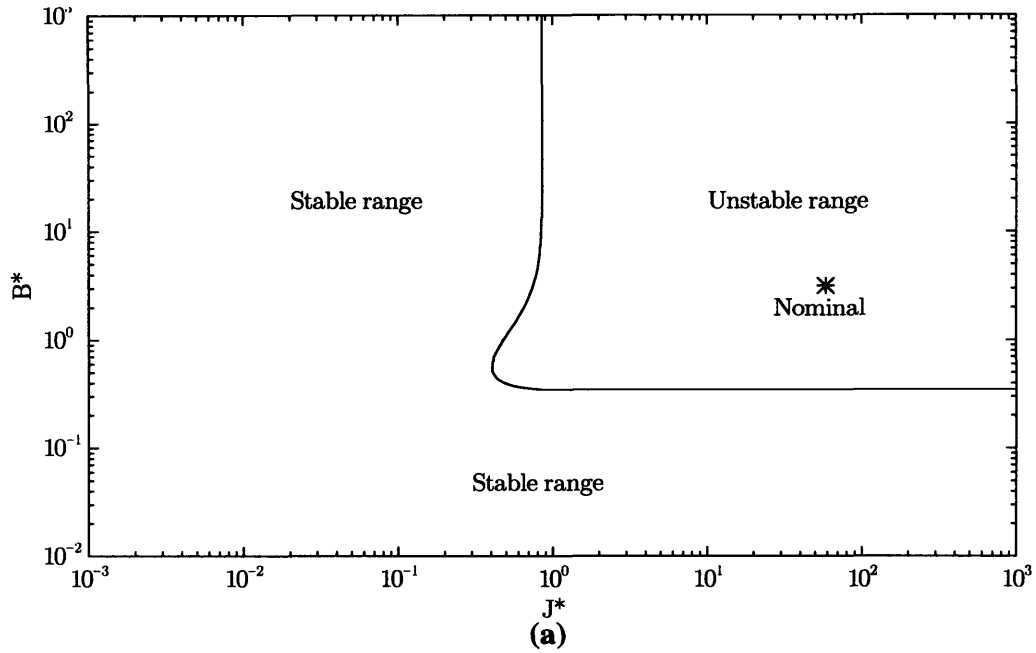
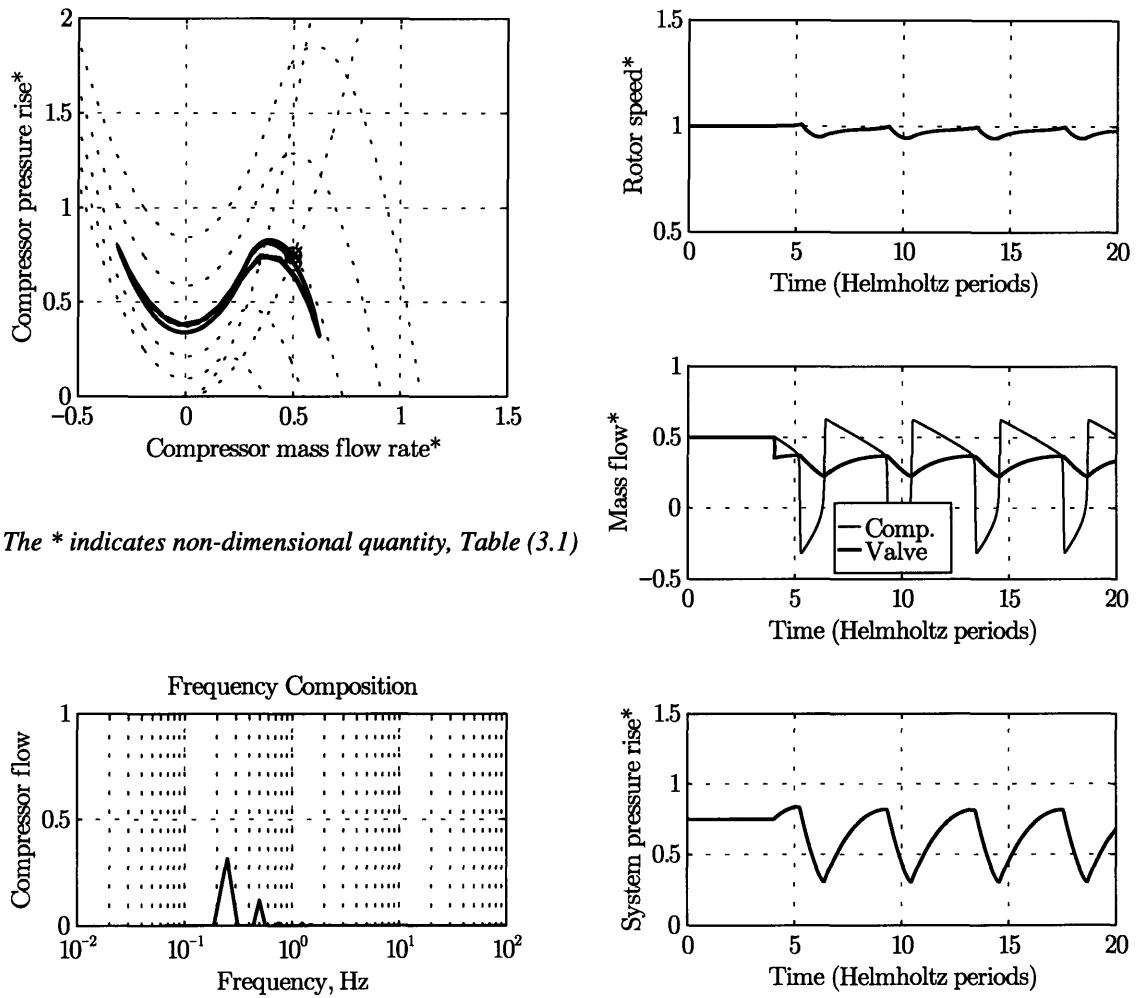
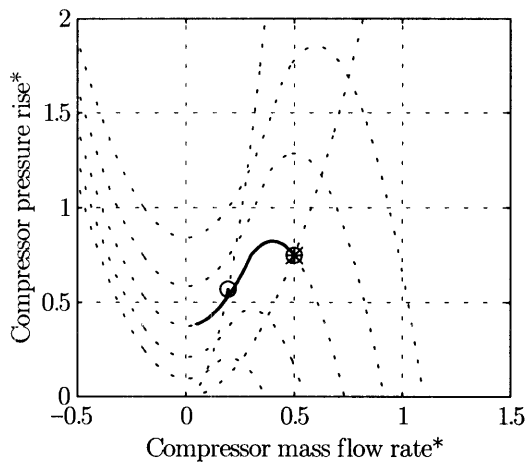


Figure (3.5) *Linear stability of base-line model: Effect of B^* and J^* . (a) for $\zeta_v = 2.0$, (b) for different values of ζ_v .*



The * indicates non-dimensional quantity, Table (3.1)

Figure (3.6) Numerical simulation: system response to a step input in $\zeta_v = 1.0$ to 2.0 at $t^* = 4.0$, system parameters: $B^* = 3.15$ and $J^* = 58.44$.



The * indicates non-dimensional quantity, Table (3.1)

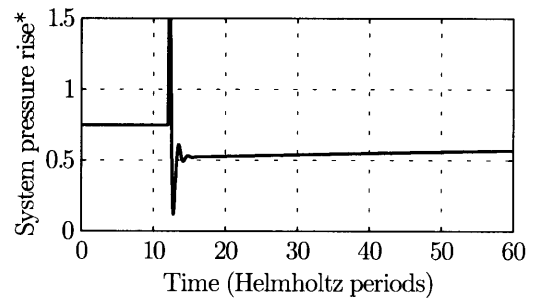
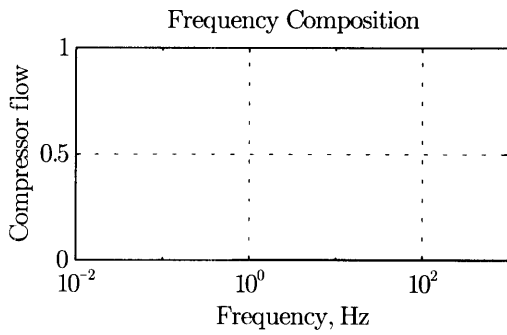
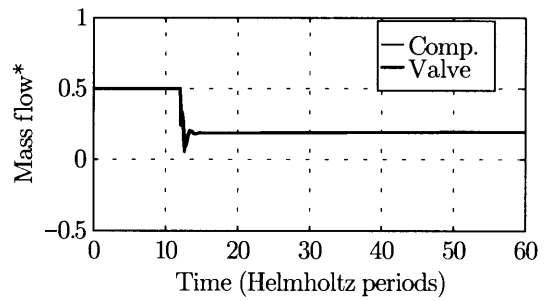
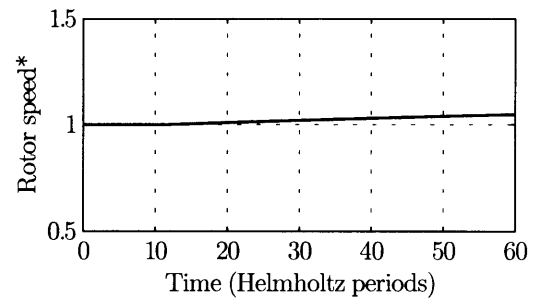


Figure (3.7) Numerical simulation: system response to a step input in $\zeta_V = 1.0$ to 5.0 , at $t^* = 4.0$, system parameters: $B^* = 0.1$ and $J^* = 58.44$.

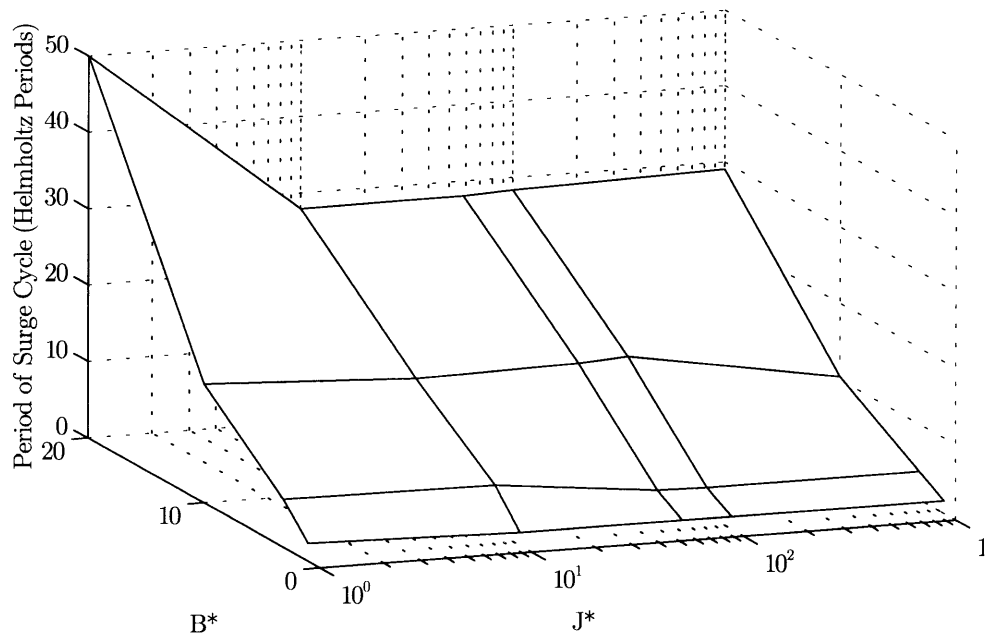


Figure (3.8) Summary of simulation results: $\zeta_v = 2.1$. Effect of B^* and J^* on post-stall period of oscillation.

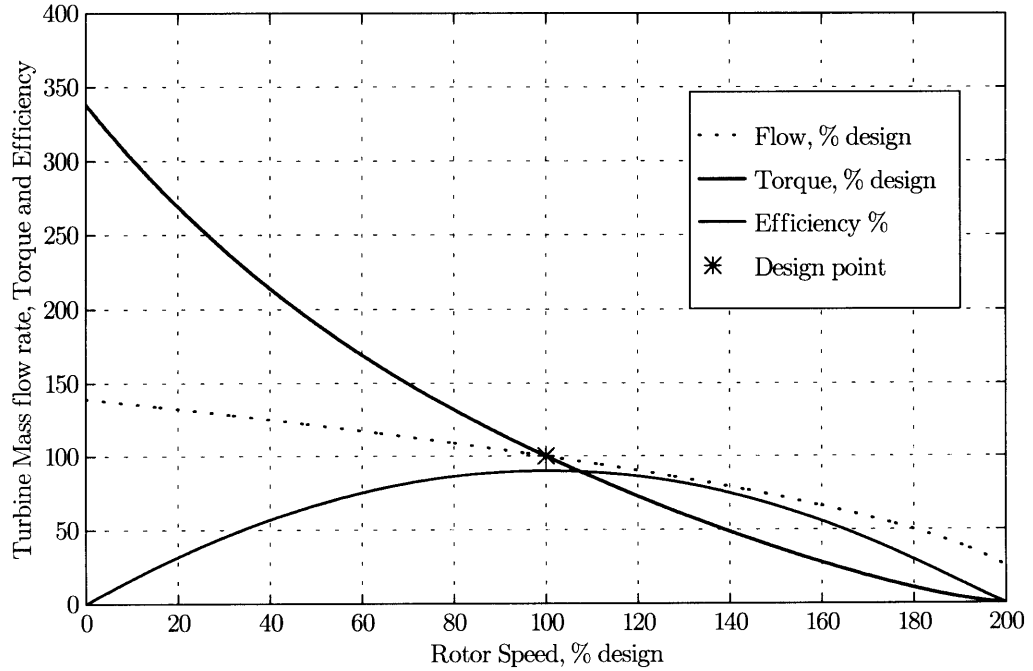


Figure (3.9) Turbine flow, torque and efficiency variation with rotor speed.

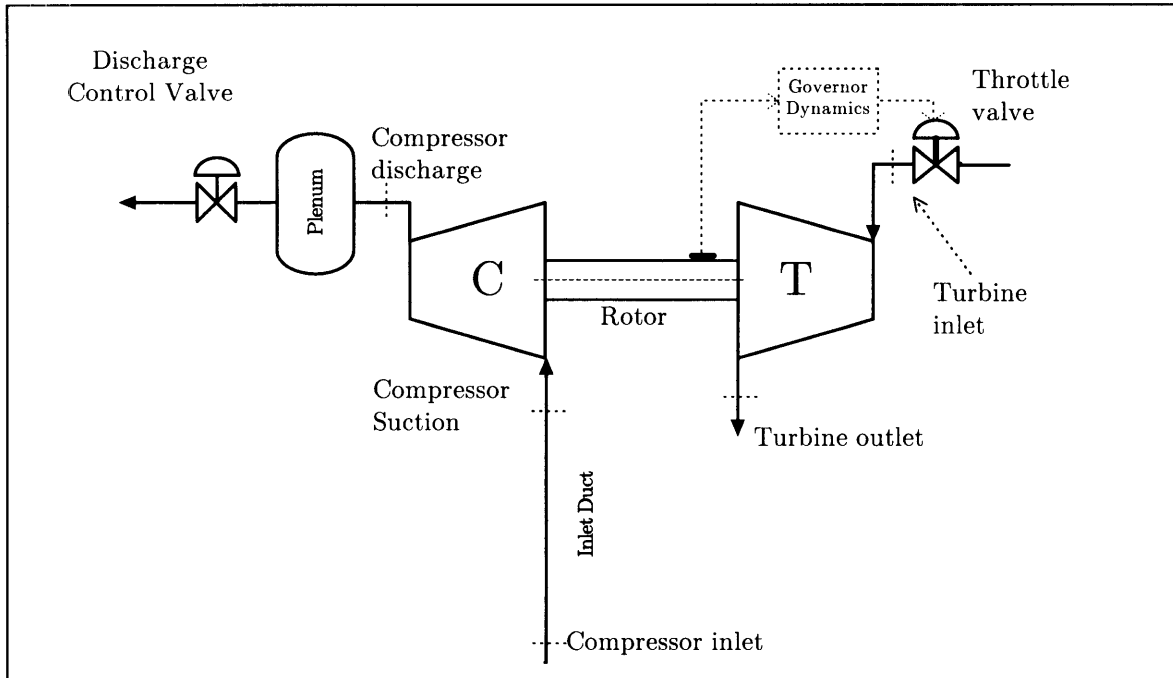
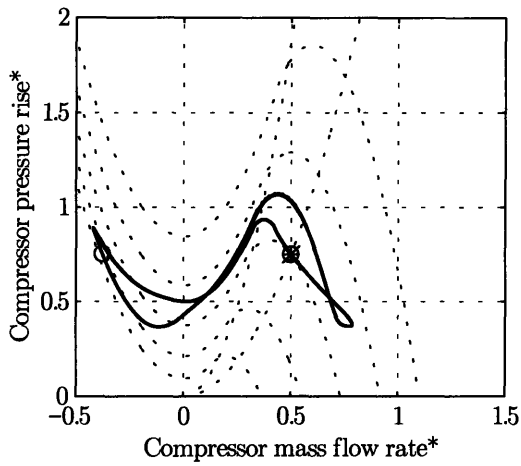


Figure (3.10) *Schematic of system with driver speed control.*



The * indicates non-dimensional quantity, Table (3.1)

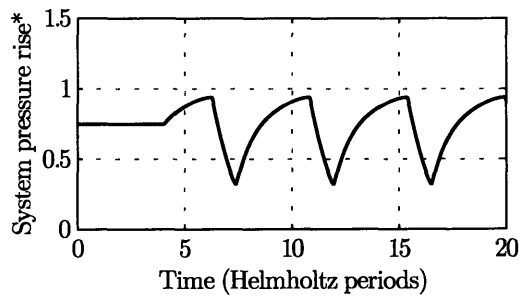
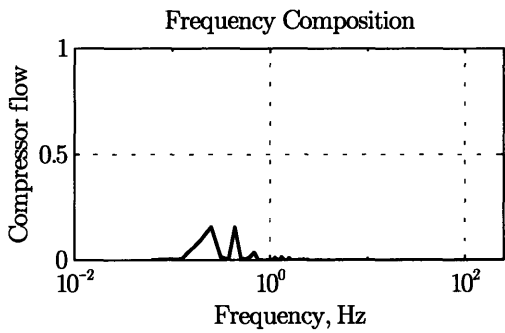
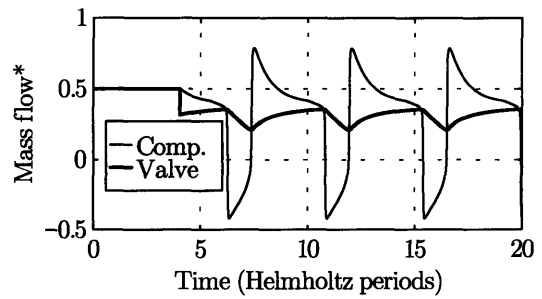
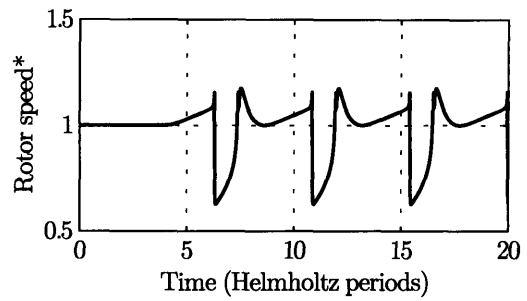
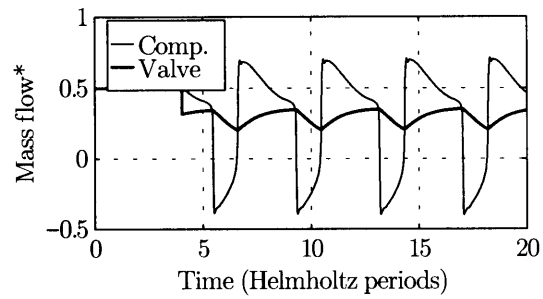
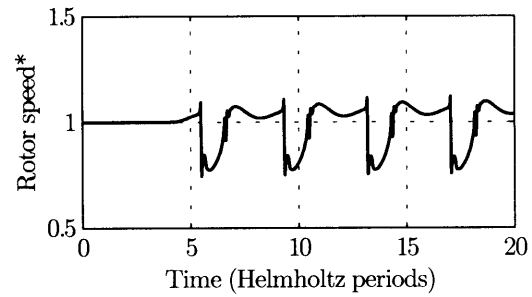
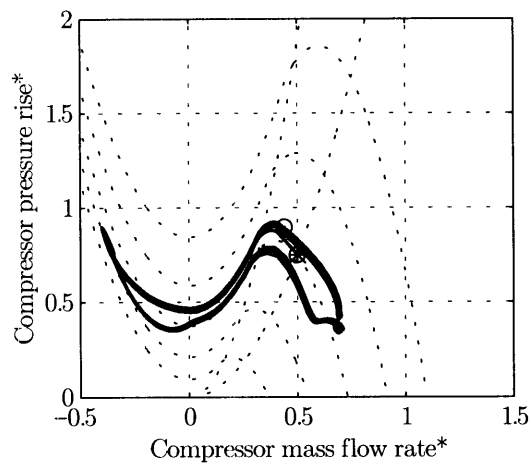


Figure (3.11) *Simulation: post-stall behavior with no speed control. Step input in $\zeta_v = 1.0$ to 2.5 , at $t^* = 4.0$, system parameters: $B^* = 3.15$ and $J^* = 0.3$.*



The * indicates non-dimensional quantity, Table (3.1)

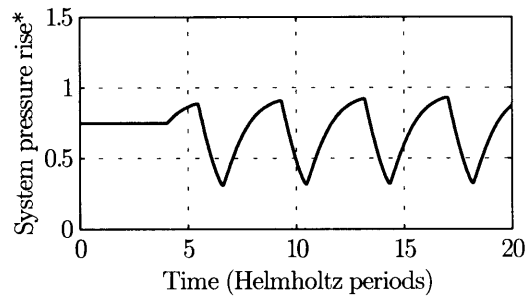
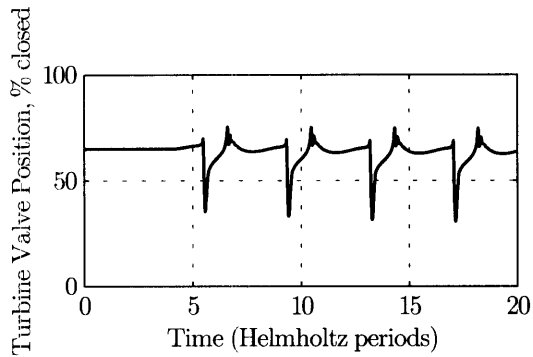
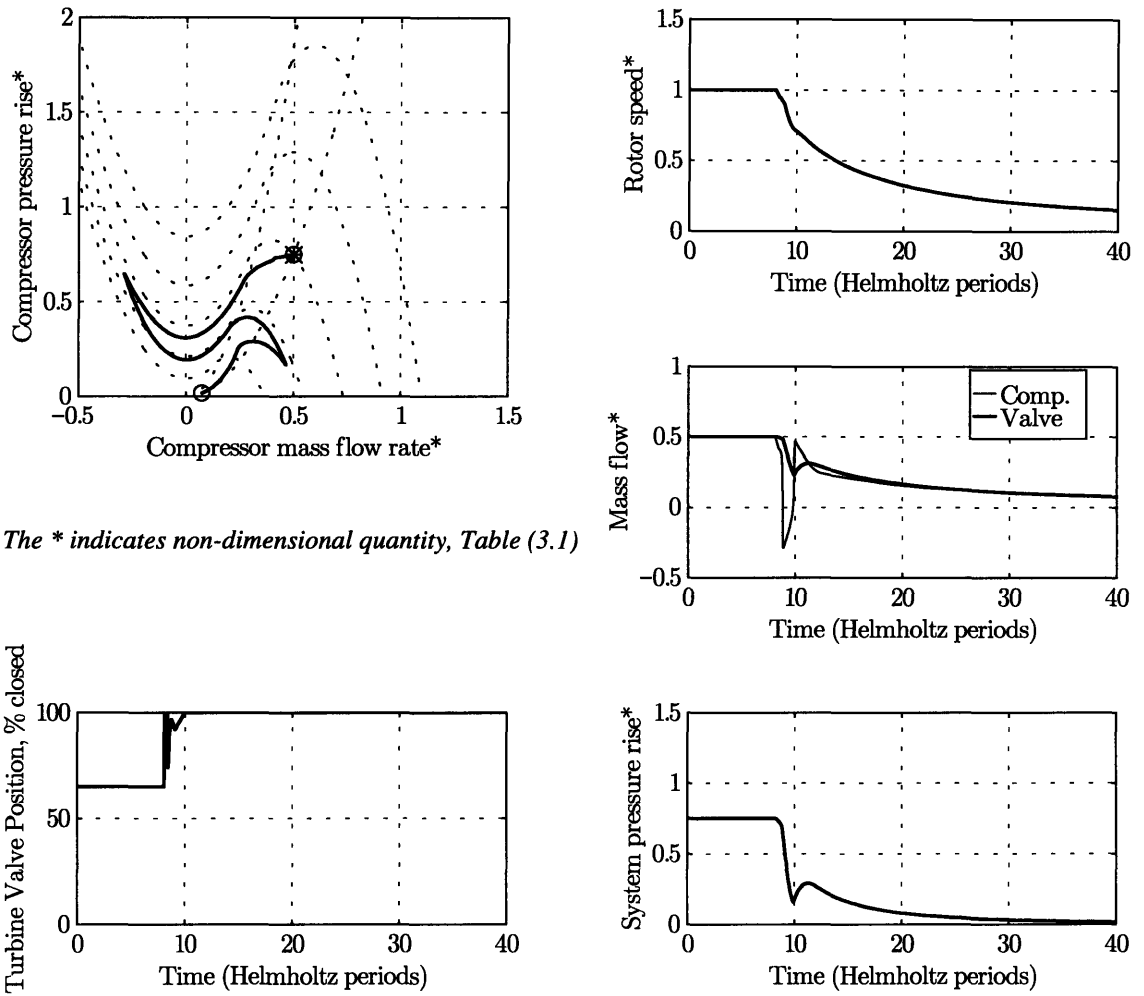
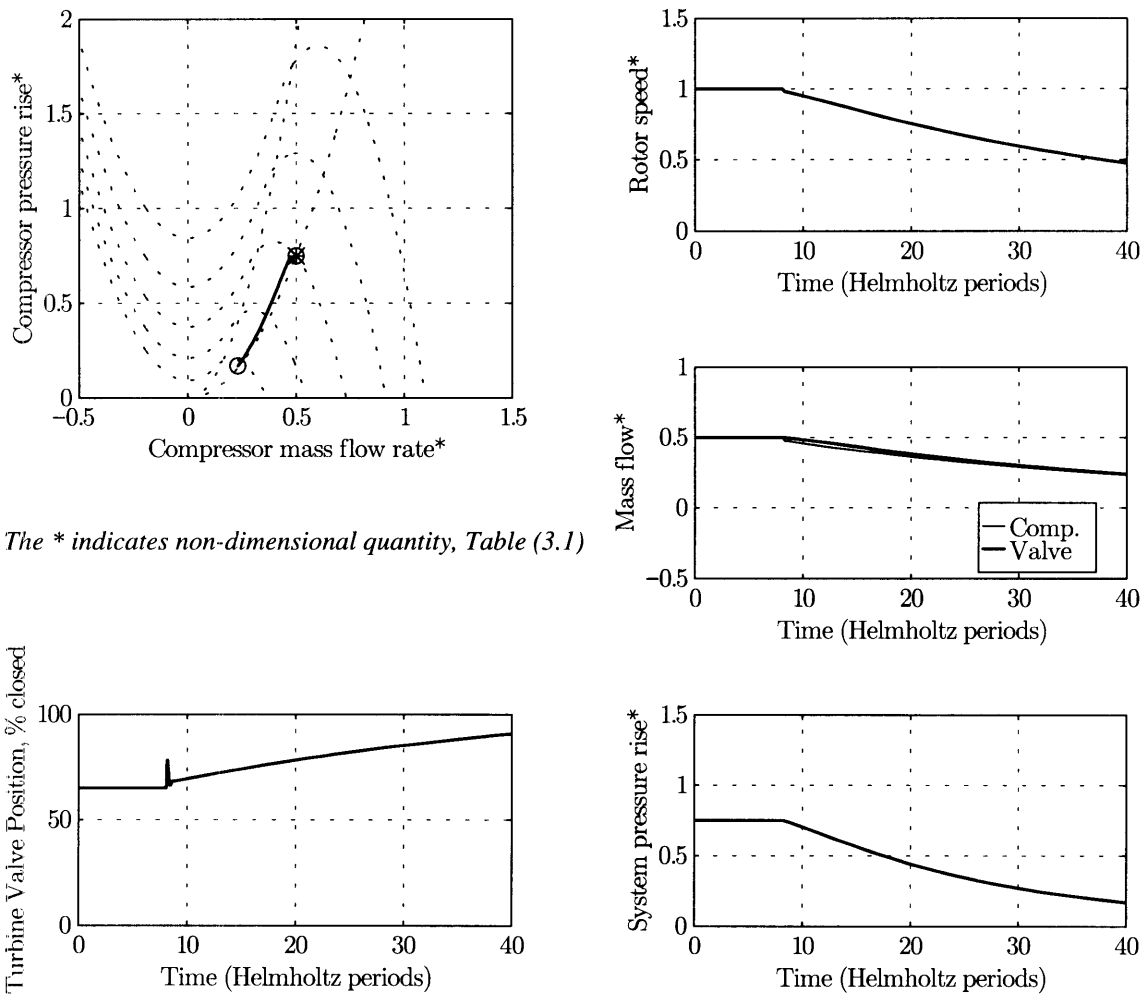


Figure (3.12) *Simulation: post-stall behavior with speed control. Step input in $\zeta_v = 1.0$ to 2.5 at , $t^* = 4.0$, system parameters: $B^* = 3.15$ and $J^* = 0.3$. Effect of speed control at small J^* .*



The * indicates non-dimensional quantity, Table (3.1)

Figure (3.13) Simulation: shut-down scenario with high value of governor gain, $K_p = 3.1$. Step input; ω_{ref} set to zero at $t^* = 8.0$. System parameters: $\zeta_v = 1$ at all times, $B^* = 3.15$, and $J^* = 29.22$.



The * indicates non-dimensional quantity, Table (3.1)

Figure (3.14) Simulation: shut-down scenario with small value of governor gain, $K_p = 0.31$. Step input; ω_{ref} set to zero at $t^* = 8.0$. System parameters: $\zeta_v = 1$ at all times, $B^* = 3.15$, and $J^* = 29.22$.

Dynamics of Typical Configuration Industrial Pumping System

This chapter addresses the role of additional components associated with typical industrial pumping systems in setting the overall dynamics. These components include the recycle line, the recycle flow control valve, the pressure control valve, and the compressor check valve. The model developed in the previous chapter is then augmented with a recycle line and the accompanying flow control valve. The significance of including the recycle loop in the model comes from the central role it plays in many current surge avoidance and recovery systems. The final model provides a means of assessing the effects of the recycle loop parameters on performing these tasks.

4.1 Typical Pumping Station: Single Compression Train

4.1.1 Control Valves and Recycle Lines

Figure (4.1) shows a schematic of a typical industrial pumping system. Three main additions can be seen in this figure as compared to Figure (3.10). A recycle loop has been added connecting the compressor discharge directly to its inlet, passing through a flow control valve. Since surge occurs at reduced compressor

flow which results from back-pressuring the compressor, providing a less resistive path for part of the compressor flow can prevent it from surging. The recycle loop specifically performs this task by opening the recycle valve upon reaching a minimum critical value of compressor flow. The penalty of this action is the waste of pumping power used to compress the recycled gas. It is of interest to both designers and operators to minimize recycling without sacrificing safety of equipment. In order to allow for a safety margin, the critical value of compressor flow that triggers the recycle valve opening is higher than that corresponding to the actual surge line of the machine, Figure (4.2). The farther these two lines are apart the less likely surge can be encountered, while the higher the recycling penalty becomes.

The second addition to this figure is the pressure control valve (indicated by the control signal from the plenum to the discharge valve). Pressure control valves are used to regulate the pressure downstream of the compressor and partially set the operating point of the system. The third addition is the check valve at the compressor discharge which is used to prevent the compressor from passing reversed flow.

4.1.2 Incorporating a Recycle Loop in the Model

The model is now expanded to include the recycle loop as shown in Figure (4.3). The following mass continuity relations can be written at the branching nodes,

$$\dot{m}_C = \dot{m}_{u,in} + \dot{m}_R \quad (4.1)$$

$$\dot{m}_{p,in} = \dot{m}_C - \dot{m}_R \quad (4.2)$$

$$\dot{m}_{p,in} = \dot{m}_{u,in} \quad (4.3)$$

where, \dot{m}_R , $\dot{m}_{p,in}$, and $\dot{m}_{u,in}$ are the mass flow rates through the recycle line, into the plenum and into the upstream duct (upstream the recycle feed) respectively.

Recycle Valve Model:

The modeling assumptions considered here are the same as those used for the compressor discharge valve. A simple quadratic constitutive relation can be written as,

$$\dot{m}_R = A_R \sqrt{\Delta p} \quad (4.4)$$

where, A_R is the recycle valve discharge coefficient, and is proportional to some equivalent flow-through area of the valve, $\Delta p = p_p - p_{u,in}$, is the system pressure rise between which the recycle valve operates. A_R would be the output of the recycle valve controller. However, to capture the dynamics of the valve in a simplified manner, it is assumed that the instantaneous value of the throttling coefficient, A_R , lags behind the controller output signal. This can be written as,

$$\tau_{lag,R} \frac{dA_R}{dt} = A_{R,s} - A_R, \quad (4.5)$$

where, $A_{R,s}$, is the controller output signal, and $\tau_{lag,R}$ is a time constant characteristic of the valve.

Recycle Loop Control Law:

A simple proportional control law is considered. The recycle valve is required to open only when the compressor flow decreases below a preset minimum. Thus, the input signal can be taken as the difference between this preset minimum and the instantaneous value of the flow. Since the minimum allowable flow depends on the speed of the compressor, it is appropriate to utilize the non-dimensionalized flow coefficient, ϕ'_C , introduced by equation (2.7). Notice that ϕ'_C is non-

dimensionalized using the instantaneous speed of the compressor. Consequently, the control law can be stated as,

$$A_{R,s} = K_R(\phi'_{C,min} - \phi'_C), \quad (4.6)$$

where, K_R is the proportional control gain, and $\phi'_{C,min}$ is a minimum flow coefficient that defines the surge protection line, and is set in a manner that guarantees an adequate safety margin from the actual surge line. Possible choices are the peak of the characteristics, which is very close to the actual surge line, or the design point at which the compressor usually operates. Implementing the latter choice results in partial recycling at any operating point to the left of the design point, while providing a reasonable safety margin.

System Governing Equations:

The model is now governed by the following state equations:

$$\frac{d\omega}{dt} = \frac{1}{J} \left[\tau_T(\omega) - \tau_C(\dot{m}_C, \omega) \right], \quad (4.7)$$

$$\frac{d\dot{m}_C}{dt} = \frac{A_u}{L_u} \left[\Delta p_C(\dot{m}_C, \omega) - \Delta p \right], \quad (4.8)$$

$$\frac{d(\Delta p)}{dt} = \frac{a^2}{V_p} \left[\dot{m}_{p,in} - \dot{m}_V(\Delta p) \right], \quad (4.9)$$

$$\dot{y}_1 = y_2, \quad (4.10)$$

$$\dot{y}_2 = -\frac{K_p}{m_G} (\omega - \omega_{ref}) - 2\zeta_G \omega_{n,G} y_2 - \omega_{n,G}^2 y_1, \quad (4.11)$$

$$\dot{y}_3 = y_1, \quad (4.12)$$

$$\frac{dA_R}{dt} = \frac{1}{\tau_{lag,R}} [A_{R,s} - A_R]. \quad (4.13)$$

The turbine throttle valve is still governed by the output equation,

$$x_t = x_{t,d} - (y_1 + T_D y_2 + \frac{1}{T_I} y_3). \quad (4.14)$$

The recycle line control logic can be described by the following relations,

$$\begin{aligned} \phi'_C &= \dot{m}_C / (\bar{\rho}_C \omega r A_u) \\ \text{if } \phi'_C &< \phi'_{C,min} \\ A_{R,s} &= K_R (\phi'_{C,min} - \phi'_C) \\ \text{else} \\ A_{R,s} &= 0 \\ \text{end} \\ \dot{m}_R &= A_R \sqrt{\Delta p} \\ \dot{m}_{p,in} &= \dot{m}_C - \dot{m}_R. \end{aligned}$$

The above set of relations defines all the new variables in the model in terms of system states and physical parameters.

4.1.3 Simulation of The Overall System

To examine the effect of the recycle loop dynamics on the overall system transient behavior, the following simulations are considered. First, the effect of the recycle valve controller gain, K_R , is examined. In all the following simulations, the system response to a step input (of fixed amplitude in all cases) in the discharge valve setting is obtained using the nominal values of B^* and J^* . Figure (4.4) shows time histories of the flow through the compressor and the recycle line using two values of K_R . The first simulation, Figure (4.4)a, demonstrates a sustained surge behavior, while in the second simulation, Figure (4.4)b, the system recovers after only one surge cycle and reaches a new steady state operating point that is char-

acterized by a slightly lower compressor flow and a typical constant recycling rate of approximately 30% of compressor flow. It has been found that for a given value of recycle valve time constant, $\tau_{lag,R}$, there is a critical value of K_R above which the system can recover from surge. In the case considered here, the value of $\tau_{lag,R}$ was 1.0 sec, for which the critical value of K_R was about 0.44.

In Figure (4.5)a, b, and c, three simulations are shown. The first two, a and b, were obtained using $\tau_{lag,R}$ value of 5.0, and K_R values of 0.2 and 0.22 respectively, and demonstrate a recovery from surge after encountering few surge cycles. It can be seen from comparing these two cases to the previous ones, that for the higher value of $\tau_{lag,R}$, a lower K_R can provide recovery. In addition, the higher value of $\tau_{lag,R}$ changed the nature of recovery in that different values of K_R caused the system to experience different number of surge cycles before fully recovering to a stable operating condition. Finally, Figure (4.5)c shows a case of surge avoidance, where the system did not experience any surge cycles. This was achieved by using a high controller gain, $K_R = 0.5$, and a very small $\tau_{lag,R} = 0.1$ (corresponding to a quick-acting valve). It should be noted that in all these simulations, the system was subjected to the same step input ($\zeta_V = 3$).

4.1.4 Discussion of Recycling Performance

Despite the success of using the recycle loop to avoid and recover form surge, there remains a question regarding the penalty involved. Two aspects of recycling-based schemes can be identified as penalizing. The first is related to the compressor condition and “health”, and the other is related to the efficiency of the overall pumping station. It is known that compressors and pumps are very sensitive to operating at reduced flow rates (with the reversed flow being the extreme). Elongated and frequent periods of operation under such conditions can

have a very strong impact on the life and the reliability of the machine. On the other hand, high levels of recycling, intended to protect the compressor, raises a concern about the efficiency of the overall pumping station.

To quantify these aspects of the recycling process, the following parameters can be introduced,

$$X_{rev} = \frac{\int_{t_1}^{t_2} [\dot{m}_C]_- dt}{\int_{t_1}^{t_2} \dot{m}_C dt}, \quad (4.15)$$

and,

$$X_{net} = \frac{\int_{t_1}^{t_2} \left[\frac{\dot{m}_V}{\bar{\rho}_C} \Delta p_C \right] dt}{\int_{t_1}^{t_2} [\tau_C \omega] dt} \quad (4.16)$$

where, X_{rev} is the ratio of (the total amount of fluid that passed through the compressor in the reversed direction) to (the net amount of fluid that passed through the compressor) during some transient t_1 to t_2 , while X_{net} is the ratio of (the useful hydraulic energy supplied to the net flow) to (the total amount of energy supplied to the compressor) during some transient t_1 to t_2 .

X_{rev} can be viewed as an indicator of how severe a transient is for the compressor. Higher values of X_{rev} indicate that the compressor was subjected to severe operating conditions during that transient in terms of reversed flow conditions. X_{net} , on the other hand, can be viewed as the efficiency of the overall pumping station averaged over some period of time. It quantifies the portion of the energy delivered to the compressor that has been used in pumping the product leaving the station. It follows that lower values of X_{rev} indicate better performance while

lower values of X_{net} indicate worse performance. These two parameters can be utilized, for example, in evaluating the performance of surge avoidance and recovery systems during a given transient scenario, or over the course of few months of normal operation.

As an application, X_{rev} and X_{net} were evaluated for the transient scenarios considered in section (4.1.3). The results are summarized in Table (4.1) . It can be noticed from these values that the last case which avoided surge completely had a zero value of X_{rev} indicating that the compressor did not experience any reversed flow. In contrast, the first case in the table had the highest X_{rev} index due to the frequent and sustained occurrence of compressor flow reversal. In the same time, the first case had the lowest X_{net} value indicating a relatively poor pumping efficiency of the overall system during the transient. All other cases, which either avoided or recovered from surge, have a relatively high pumping efficiency index.

Reference Figure	X_{rev}	X_{net}	Note
Figure (4.4)a	0.068	0.550	sustained surge oscillations, no recovery
Figure (4.4)b	0.004	0.750	recovery after one surge cycle
Figure (4.5)a	0.027	0.764	recovery after three surge cycles
Figure (4.5)b	0.016	0.781	recovery after two surge cycles
Figure (4.5)c	0	0.755	surge was avoided

Table (4.1) *Summary of recycle loop performance indices.*

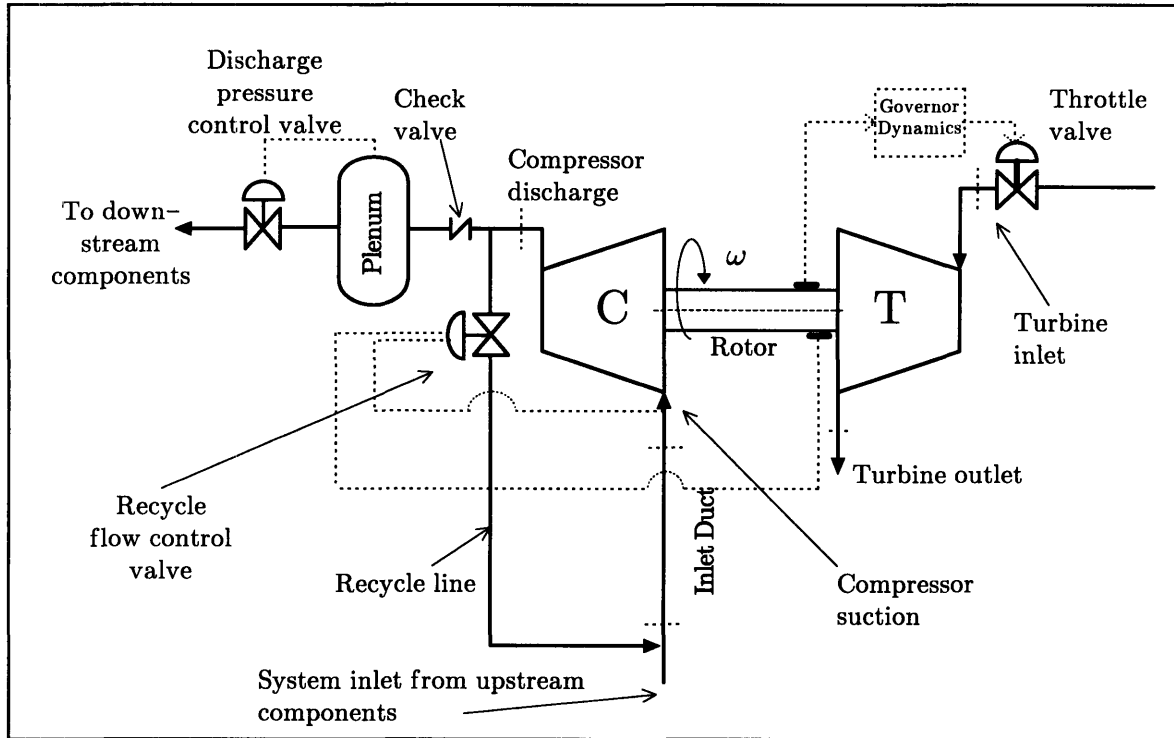


Figure (4.1) *Typical configuration of industrial pumping station: single compression train.*

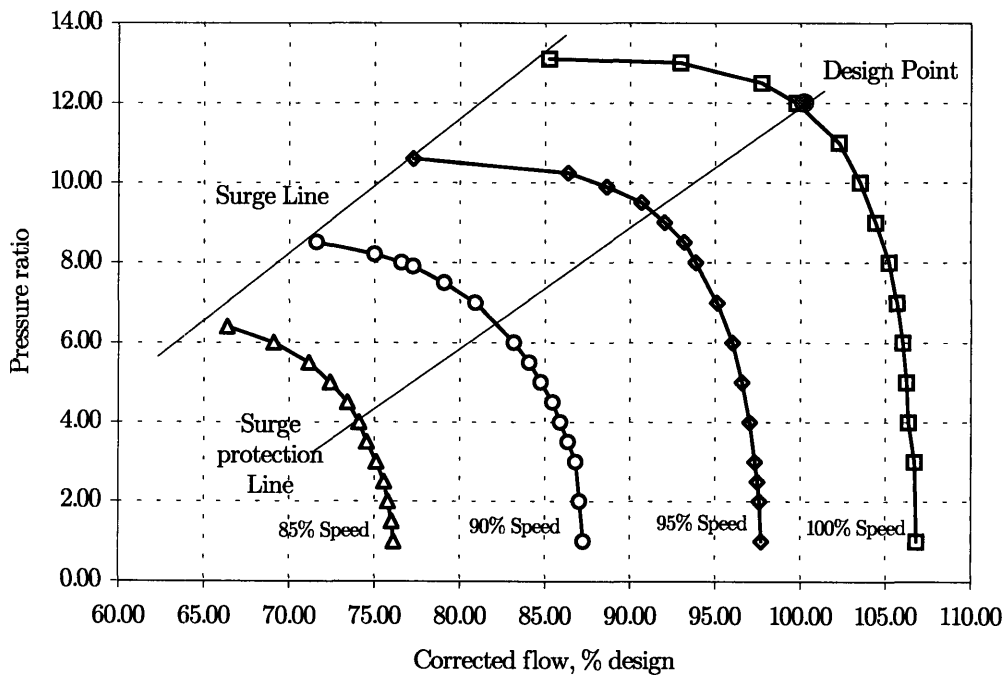


Figure (4.2) *Typical compressor characteristic map showing the surge line and the safety line used to avoid surge.*

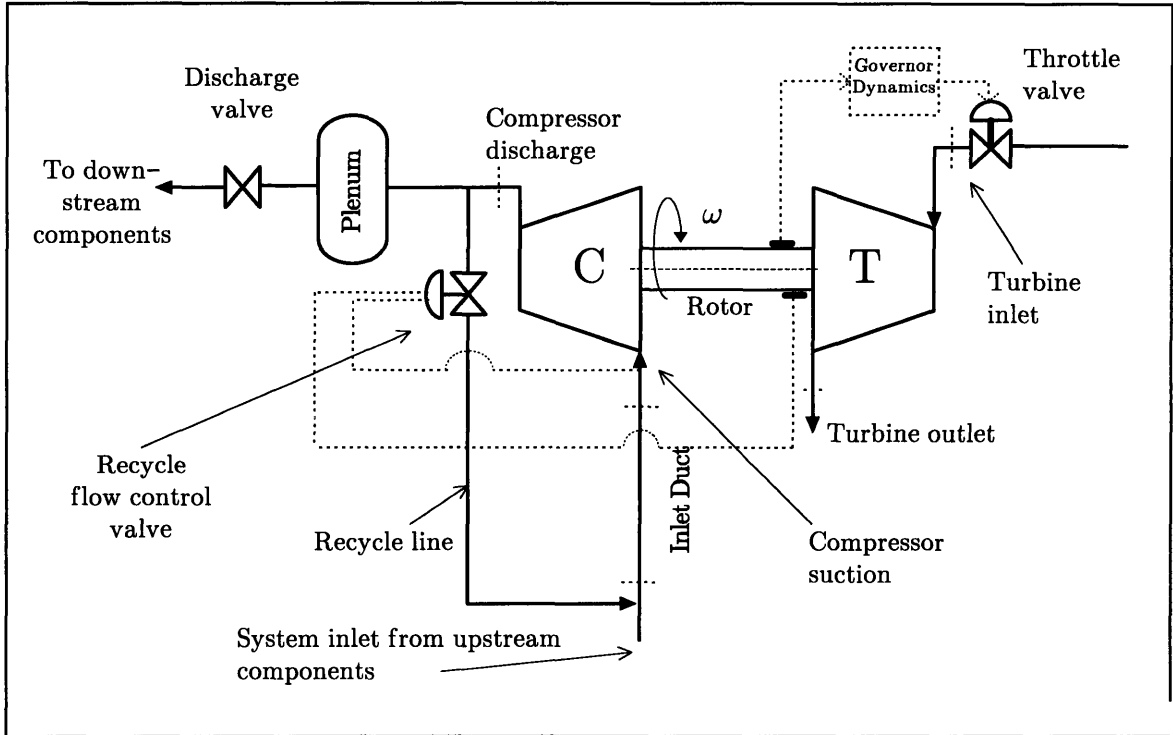


Figure (4.3) Schematic of model incorporating a recycle loop.

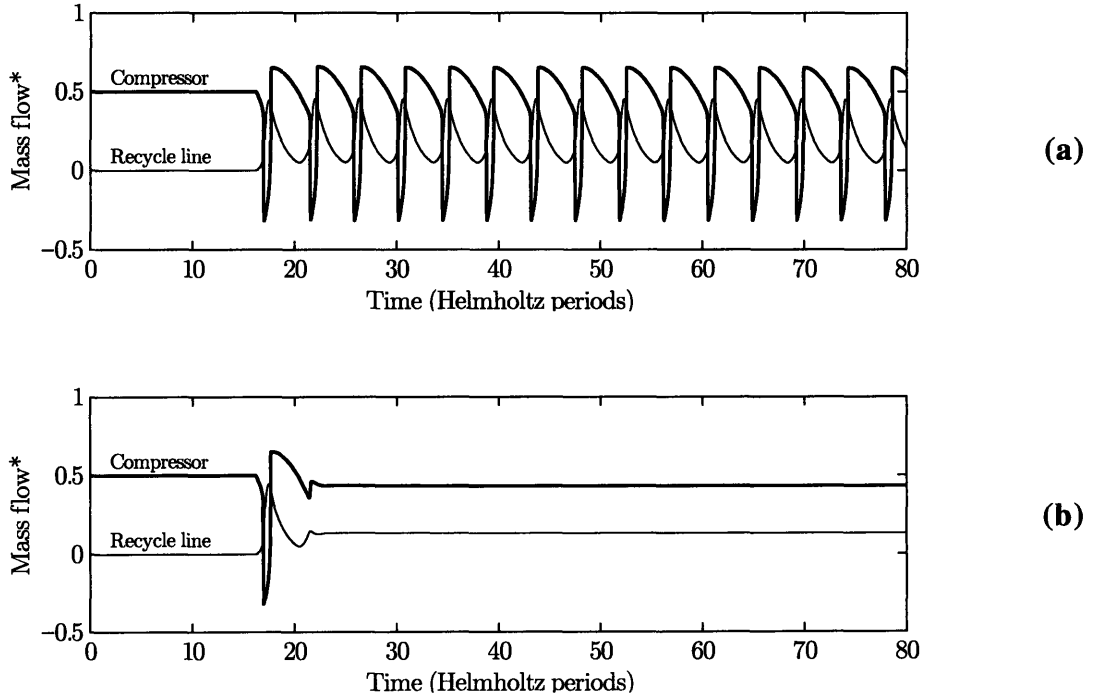
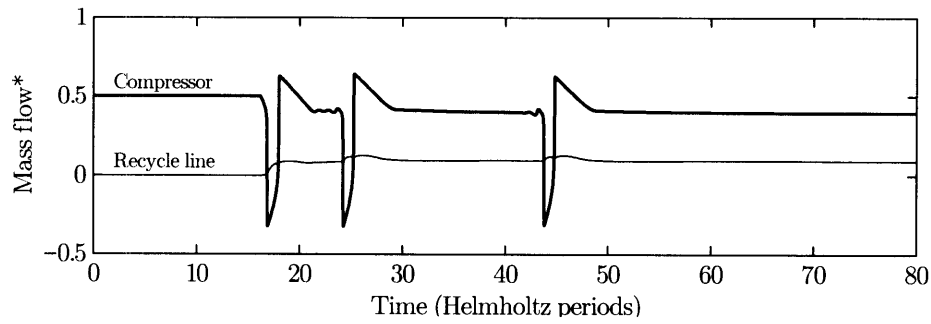
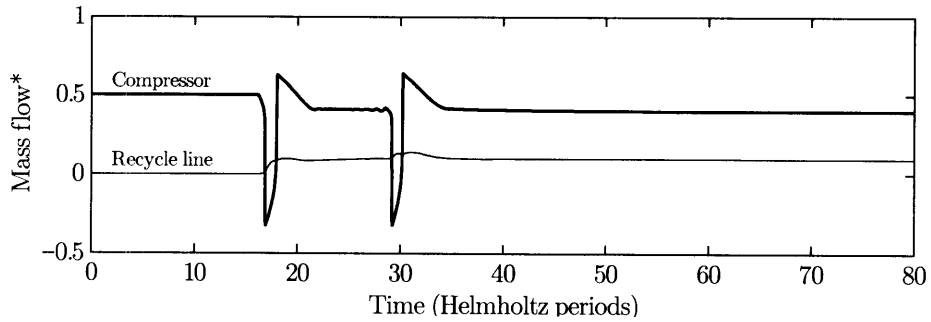


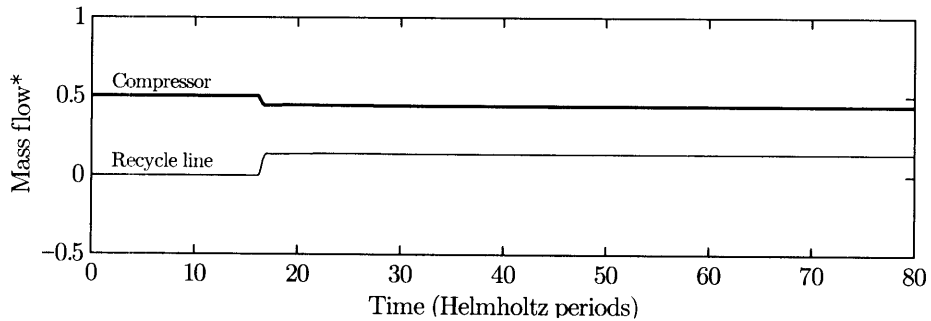
Figure (4.4) Simulation: model with recycle loop. Effect of K_R . (a) $K_R = 0.436$. (b) $K_R = 0.437$.



(a)



(b)



(c)

Figure (4.5) *Simulation: model with recycle loop. Effect of $\tau_{lag,R}$. (a) $\tau_{lag,R} = 5$, $K_R = 0.2$. (b) $\tau_{lag,R} = 5$, $K_R = 0.22$. (c) $\tau_{lag,R} = 0.1$, $K_R = 0.5$.*

Summary and Conclusions

5.1 Summary and Conclusions

In this study, existing models of basic compression systems were expanded to capture the dynamics of industrial pumping systems. Compared to basic compression systems, industrial applications are characterized by having additional components, being associated with specific operational requirements, and being integrated into complex networks of other sub-systems. The models developed in this study are intended to facilitate the prediction and control of their transient behavior.

The work presented in this thesis can be summarized as follows.

Modeling:

- A series of models that capture the dynamics of interest in industrial pumping systems have been developed.
- These models incorporated, at different stages, a industrial driver model including its speed control subsystem, and a compressor recycle loop. They also incorporated full range, realistic constitutive relations of critical components.

- A few modeling assumptions and practical considerations were evaluated in the context of industrial pumping systems.
- These models were used to predict and quantify the system instability onset limits, the post-stall behavior, and the effect of critical subsystems on the dynamics of the overall system.
- The models were also utilized in explaining the physics associated with such dynamics.

Results and Analysis:

- Using the base-line model of a simple pumping system, it was shown that both the instability onset limit and the post-stall behavior (surge dynamics) depend on two non-dimensional parameters, B^* and J^* . The first being proportional to the ratio of effective fluid compliance to effective fluid inertia, where the second is proportional to the ratio of the effective mechanical inertia to effective fluid inertia.
- The instability onset limit was found to strongly depend on B^* , such that lower values of B^* corresponded to a wider stable range of operation. In contrast, smaller values of J^* had a stabilizing effect that was limited to a narrower range of operation. It was shown that there is a critical value of discharge throttling beyond which the stability limit becomes mostly dependent on B^* .
- The stabilizing effect of rotor speed fluctuations was explained using the model. It was found that at the point where the dynamic instability initiates, the variation in rotor speed effectively produces a less positive compressor slope.

- The post-stall behavior of the system was found to be mainly influenced by B^* , such that higher values of B^* resulted in surge oscillations of higher periods. The effect of J^* on surge period was only pronounced at high B^* , where higher values of J^* reduced the surge period.
- The inclusion of the turbine speed control subsystem was found to have a significant impact on large transients. The governor controller gain was found to play a critical role in a shut-down scenario by either causing the system to encounter a surge cycle or avoid it. The effect of high controller gain on post-stall behavior was pronounced only with small J^* , and was found to: reduce the amplitude of rotor speed oscillations, reduce the surge period, and develop earlier instability, leading to the conclusion that high controller gain can be thought of as a higher equivalent J^* .
- The simple model used for including the recycle line was able to capture the main dynamics of surge avoidance and recovery. The ability of the recycle line to achieve this depended on the controller gain and the time lag constant associated with the recycle valve dynamics.
- Two parameters were introduced to quantify the effectiveness and efficiency of the recycle line in avoiding and recovering from surge. The first was based on the amount of reversed flow through the compressor, and the second was based on the amount of energy used to deliver the net useful product.

5.2 Recommendations For Future Research

Several additional aspects of modeling and analyzing the dynamics of industrial pumping systems can be identified as areas of interest and practical import.

- The task of extracting the equivalent parameters of fluid inertia, damping and compliance from a real industrial installation is non-trivial. Examining actual components, such as process columns and control valves, and establishing a methodology to estimate their dynamic character can improve the practical value of the model.
- The models developed in this study require the constitutive relations of the compressor as an input, upon which the success of the model largely depends. Industrial multi-stage compressor performance data is usually based on testing of the specific machine and does not include the post-stall portion of the characteristics. The ability to predict this part of the characteristics based on understanding the physics of the flow instability in this class of machines is of great value.
- Further analysis of the models developed so far utilizing the analytical and numerical tools available from Non-linear Dynamics Theory, such as bifurcation analysis, can potentially reveal more about the physics of these systems and assist in altering their non-linear behavior in a rigorous fashion. This approach has already been taken by many researchers in analyzing basic, low order pumping systems, and complex high order dynamic systems.
- The analytical results presented in this study or produced by similar models need to be compared to transient experimental data. Such data is not readily available. The instrumentation commonly installed in industry is suited for monitoring daily operation and does not have the time resolution needed to collect transient data. An experimental effort aimed at acquiring

transient data for an industrial pumping system in a typical installation would facilitate verifying the model, its assumptions and results.

- Utilizing these models, existing surge avoidance schemes can be assessed and compared. New control concepts, including active suppression of compressor instabilities, can also be examined in the context of industrial pumping systems.
- The interaction of many pumping systems should be considered. A unified modeling notation, such as Bond Graphs, can be utilized to automate the construction, simulation and analysis of complex models representing integrated process plants.
- Ultimately, a computer-based technology can be developed such that it provides design, operations, and control decisions based on the dynamic models of these complex industrial applications.

References

- [1] Abed, E.H., Houpt, P.K., and Hosny, W.M., “Bifurcation Analysis of Surge and Rotating Stall in Axial Flow Compressors,” *Trans. ASME Journal of Turbomachinery*, Vol. 115, October 1993, pp. 817–824.
- [2] Cox, H.R. (Consulting Editor), “*Gas Turbine Principles and Practice*,” George Newnes (1955).
- [3] Cumpsty, N.A., “*Compressor Aerodynamics*,” Longman (1989).
- [4] Dixon, S.L., “*Fluid Mechanics, Thermodynamics of Turbomachinery*,” Pergamon (1989).
- [5] Emmons, H.W., Pearson, C.E., and Grant, H.P., “Compressor Surge and Stall Propagation,” *Trans. ASME*, Vol. 79, April 1955, pp. 455–469.
- [6] Epstein, A.H., Ffowcs, F.E., and Greitzer, E.M., “Active Suppression of Compressor Instabilities,” AIAA–86–1994, July 1986.
- [7] Fink, D.A., “Surge Dynamics and Unsteady Phenomena in Centrifugal Compressors,” Massachusetts institute of Technology – Gas Turbine Laboratory, Technical Report 193, June 1988.
- [8] Gamache, R.N., and Greitzer, E.M., “Reverse Flow in Multistage Axial Compressors,” AIAA–86–1747, June 1986.
- [9] Greitzer, E.M., “The Stability of Pumping Systems—The 1980 Freeman Scholar Lecture,” *Trans. ASME Journal of Fluids Engineering*, Vol. 103, June 1981, pp. 193–242.
- [10] Greitzer, E.M., “Surge and Rotating Stall in Axial Compressors, Part I: Theoretical Compression System Model,” *Trans. ASME Journal of Engineering for Power*, Vol. 98, No. 2, April 1976, pp. 190–198.
- [11] Greitzer, E.M., “Surge and Rotating Stall in Axial Compressors, Part II: Experimental Results and Comparison with Theory,” *Trans. ASME Journal of Engineering for Power*, Vol. 98, No. 2, April 1976, pp. 199–217.

- [12] Gysling, D.L., Dugundji, J., Greitzer, E.M., and Epstein, A.H., "Dynamics Control of Centrifugal Compressor Surge Using Tailored Structures," *Journal of Turbomachinery*, Vol. 113, April 1991, pp. 710–722.
- [13] Horlock, J.H., "Axial Flow Compressors," Krieger (1958).
- [14] Horlock, J.H., "Axial Flow Turbines," Krieger (1973).
- [15] Karnopp, D.C., Margolis, D.L., and Rosenberg, R.C., "System Dynamics: A Unified Approach," John Wiley & Sons, Second Edition (1990).
- [16] Kerrebrock, J.L., "Aircraft Engines and Gas Turbines," The MIT Press (1992).
- [17] McNulty, G.S., "A Study of Dynamic Compressor Surge Control Strategies for a Gas Turbine Engine," M.S. Thesis, Department of Aeronautics and Astronautics, MIT, September 1993.
- [18] Ogata, K., "Modern Control Engineering," Prentice–Hall (1990).
- [19] Paynter, H.M., "The Dynamics and Control of Eulerian Turbomachines," *Trans. ASME Journal of Dynamic Systems, Measurements, and Control*, Sept. 1972, pp. 198–205.
- [20] Rowen, W.I., "Simplified Mathematical Representation of Heavy–Duty Gas Turbines," *Trans. ASME Journal of Engineering for Power*, Vol. 105, October 1983, pp. 865–869.
- [21] Rowen, W.I., "Simplified Mathematical Representation of Single Shaft Gas Turbines in Mechanical Drive Service," *Turbomachinery International*, July/August 1992, pp. 26–32.
- [22] Salisbury, J.K., "Steam Turbines and Their Cycles," Krieger Publishing Company (1950).
- [23] Simon, J.S., "Feedback Stabilization of Compression Systems," Massachusetts Institute of Technology – Gas Turbine Laboratory, Technical Report 216, March 1993.
- [24] Stodola, A., "Steam and Gas Turbines," Vol. 1: Peter Smith (1945), Vol. 2: McGraw–Hill (1927).

- [25] Strang, G., "Introduction to Applied Mathematics," Wellesley-Cambridge (1986).
- [26] Wilson, D.G., "The Design of High-Efficiency Turbomachinery and Gas Turbines," The MIT Press (1989).
- [27] Wylen, G.J., Sonntag, R.E., and Borgnakke, C., "Fundamentals of Classical Thermodynamics," John Wiley & Sons (1994).